Rheological constitutive equation for a model of soft glassy materials

Peter Sollich*
Department of Physics, University of Edinburgh, Edinburgh EH9 3JZ, United Kingdom
(Received 1 December 1997)

We solve exactly and describe in detail a simplified scalar model for the low frequency shear rheology of foams, emulsions, slurries, etc. [P. Sollich, F. Lequeux, P. Hébraud, and M. E. Cates, Phys. Rev. Lett. **78**, 2020 (1997)]. The model attributes similarities in the rheology of such ''soft glassy materials'' to the shared features of structural disorder and metastability. By focusing on the dynamics of mesoscopic elements, it retains a generic character. Interactions are represented by a mean-field noise temperature x, with a glass transition occurring at $x=1$ (in appropriate units). The exact solution of the model takes the form of a constitutive equation relating stress to strain history, from which all rheological properties can be derived. For the linear response, we find that both the storage modulus G' and the loss modulus G'' vary with frequency as ω^{x-1} for $1<x<2$, becoming flat near the glass transition. In the glass phase, aging of the moduli is predicted. The steady shear flow curves show power-law fluid behavior for $x<2$, with a nonzero yield stress in the glass phase; the Cox-Merz rule does not hold in this non-Newtonian regime. Single and double step strains further probe the nonlinear behavior of the model, which is not well represented by the Bernstein-Kearseley-Zapas relation. Finally, we consider measurements of G' and G'' at finite strain amplitude γ. Near the glass transition, G'' exhibits a maximum as γ is increased in a strain sweep. Its value can be strongly overestimated due to nonlinear effects, which can be present even when the stress response is very nearly harmonic. The largest strain γ_c at which measurements still probe the linear response is predicted to be roughly frequency independent. [S1063-651X(98)04407-9]

PACS number(s): 83.20.−d, 83.70.Hq, 05.40.+j

I. INTRODUCTION

Many soft materials, such as foams, emulsions, pastes, and slurries, have intriguing rheological properties. Experimentally, there is a well-developed phenomenology for such systems: their nonlinear flow behavior is often fit to the form $\sigma=A+B\dot{\gamma}^n$ where σ is shear stress and $\dot{\gamma}$ strain rate. This is the Herschel-Bulkeley equation [1,2]; or (for $A=0$) the ''power-law fluid'' [1–3]. For the same materials, linear or quasilinear viscoelastic measurements often reveal storage and loss moduli $G'(\omega)$, $G''(\omega)$ in nearly constant ratio (G''/G' is usually about 0.1) with a frequency dependence that is either a weak power-law (clay slurries, paints, microgels) or negligible (tomato paste, dense emulsions, dense multilayer vesicles, colloidal glasses) [4–10]. This behavior persists down to the lowest accessible frequencies (about $10^{-3}-1$ Hz depending on the system), in apparent contradiction to linear response theory, which requires that $G''(\omega)$ should be an odd function of ω. This behavior could in principle be due to slow relaxation modes below the experimentally accessible frequency range (see Fig. 1). Each of those would cause a drop in $G'(\omega)$ and a bump in $G''(\omega)$ as the frequency is tracked downward. However, where the search for system specific candidates for such slow modes has been carried out (for the case of foams and dense emulsions, for example, see [11]), it has not yielded viable candidates; it therefore seems worthwhile to look for more generic explanations of the observed behavior.

Indeed, the fact that similar anomalous rheology should be seen in such a wide range of soft materials suggests a common cause. In particular, the frequency dependence indicated above points strongly to the generic presence of slow ''glassy'' dynamics persisting to arbitrarily small frequencies. This feature is found in several other contexts [12–14], such as the dynamics of elastic manifolds in random media [15,16]. The latter is suggestive of rheology: charge density waves, vortices, contact lines, etc. can ''flow'' in response to an imposed ''stress.''

In a previous letter [17] it was argued that glassy dynamics is a natural consequence of two properties shared by all the soft materials mentioned above: *structural disorder* and *metastability*. In such ''soft glassy materials'' (SGMs), thermal motion alone is not enough to achieve complete structural relaxation. The system has to cross energy barriers (for

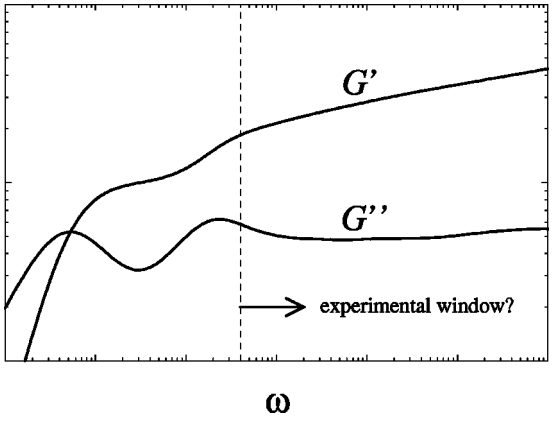

FIG. 1. Sketch of frequency dependence of linear moduli, showing possible slow relaxation modes at frequencies below the measurement window.

*Electronic address: P.Sollich@ed.ac.uk

example, those associated with rearrangement of droplets in an emulsion) that are very large compared to typical thermal energies. It therefore adopts a disordered, metastable configuration even when (as in a monodisperse emulsion or foam) the state of least free energy would be ordered [18]. The importance of structural disorder has previously been noted in more specific contexts [7,11,19–23], but its unifying role in rheological modeling can be more easily appreciated by focusing on the class of SGMs as a whole.

In Ref. [17], a minimal, scalar model for the generic rheology of SGMs was introduced, which incorporates the above ideas. We refer to this model as the ''soft glassy rheology'' (SGR) model in the following. The main contribution of the present publication is the exact solution of this model; at the same time, we also provide more detailed analytical and numerical support for the results announced in [17]. The exact solution is in the form of a constitutive equation relating the (shear) stress at a given time to the strain history. We use this to study a range of linear and nonlinear rheological properties of the model; qualitative comparisons with experimental data show that these capture many generic rheological characteristics of SGMs. We do not attempt more quantitative fits to experimental data for specific materials because the model in its present form is almost certainly too oversimplified for this purpose. We do, however, hope to carry out a more quantitative study in future work, once the remaining ambiguities in the interpretation of the model parameters (see Sec. VI) have been clarified and some of the improvements suggested in Sec. VII have been incorporated into the model.

We introduce the SGR model in Sec. II, along with Bouchaud's glass model on which it builds. Section III contains our main result, the constitutive equation. Its predictions in the linear response regime are discussed in Sec. IV, while in Sec. V we analyze several nonlinear scenarios including steady shear flow, shear startup, large step strains, and large oscillatory strains. The physical significance and interpretation of the various parameters of the SGR model are not obvious; in Sec. VI we discuss in more detail the ''noise temperature'' x and ''attempt frequency'' Γ_0 of the model. Our results are summarized in Sec. VII.

II. THE SGR MODEL

The SGR model is a phenomenological model that aims to explain the main features of SGM rheology (both linear and nonlinear) as described above. To apply to a broad range of materials, such a model needs to be reasonably generic. It should therefore incorporate only a minimal number of features common to all SGMs, leaving aside as much system specific detail as possible. One important feature is the ''glassiness,'' i.e., the effects of structural disorder and metastability. We model this using a fairly intuitive picture of a glass: it consists of local ''elements'' (we will be more specific later about what we mean by these in the context of SGMs) that are trapped in ''cages'' formed by their neighbors so that they cannot move. Occasionally, however, a rearrangement of the elements may be possible, due to thermal activation, for example. Glass models of this kind are commonly referred to as ''trap models'' and have been studied by a large number of authors (see, e.g., Refs. [13,24–30]). An alternative to such models would be, for example, mode-coupling theories [31,32], which, at least in their simplest form, neglect all (thermally) activated processes. We prefer trap models for our purposes, because they are simpler and also generally more physically transparent [33].

A. Bouchaud's glass model

Bouchaud formalized the above intuitive trap picture of a glass into a one-element model [12,13]: an individual element ''sees'' an energy landscape of traps of various depths E; when activated, it can ''hop'' to another trap. Bouchaud assumed that such hopping processes are due to thermal fluctuations. In SGMs, however, this is unlikely as $k_B T$ is very small compared to typical trap depths E (see Sec. VI). The SGR model assumes instead that the ''activation'' in SGMs is due to it *interactions*: a rearrangement somewhere in the material can propagate and cause rearrangements elsewhere. In a mean-field spirit, this coupling between elements is represented by an *effective temperature* (or noise level) x. This idea is fundamental to the SGR model.

The equation of motion for the probability of finding an element in a trap of depth E at time t is [12,13,34]

$$\frac{\partial}{\partial t}P(E,t) = -\Gamma_0 e^{-E/x}\, P(E,t) + \Gamma(t)\, \rho(E). \qquad (1)$$

In the first term on the right-hand-side (rhs), which describes elements hopping out of their current traps, Γ_0 is an attempt frequency for hops, and $\exp(-E/x)$ is the corresponding activation factor. The second term represents the state of these elements directly after a hop. Bouchaud made the simplest possible assumption that the depth of the new trap is completely independent of that of the old one; it is simply randomly chosen from some ''prior'' distribution of trap depths $\rho(E)$. The rate of hopping into traps of depth E is then $\rho(E)$ times the overall hopping rate, given by

$$\Gamma(t) = \Gamma_0 \langle e^{-E/x} \rangle_P = \Gamma_0 \int dE\, P(E,t) e^{-E/x}. \qquad (2)$$

Bouchaud's main insight was that the model (1) can describe a glass transition *if the density of deep traps has an exponential tail*, $\rho(E) \sim \exp(-E/x_g)$, say. Why is this? The steady state of Eq. (1), if one exists, is given by $P_{\rm eq}(E) \propto \exp(E/x)\rho(E)$; the Boltzmann factor $\exp(E/x)$ (no minus here because trap depths are measured from zero *downwards*) is proportional to the average time spent in a trap of depth E. At $x = x_g$, it just cancels the exponential decay of $\rho(E)$, and so the supposed equilibrium distribution $P_{\rm eq}(E)$ tends to a constant for large E; it is not normalizable. This means that, for $x \leqslant x_g$, the system does not have a steady state; it is (''weakly'') nonergodic and ''ages'' by evolving into deeper and deeper traps [12,13]. The model (1) therefore has a *glass transition* at $x = x_g$.

With Bouchaud's model, we have a good candidate for describing in a relatively simple way the glassy features of SGMs. Its disadvantages for our purposes are as follows: (i) The assumption of an exponentially decaying $\rho(E)$ is rather arbitrary in our context. It can be justified in systems with ''quenched'' (i.e., fixed) disorder, such as spin glasses, using extreme value statistics (see, e.g., [35]), but it is not obvious

how to extend this argument to SGMs. (ii) The exponential form of the activation factor in Eq. (1) was chosen by analogy with thermal activation. But for us, x describes effective noise arising from interactions, so this analogy is by no means automatic, and functional forms other than exponential could also be plausible. In essence, we view (i) *together with* (ii) as a phenomenological way of describing a system with a glass transition.

B. Incorporating deformation and flow

To describe deformation and flow, the SGR model [17] incorporates strain degrees of freedom into Bouchaud's glass model. A generic SGM is conceptually subdivided into a large number of *mesoscopic regions*, and these form the ''elements'' of the model. By mesoscopic we mean that these regions must be (i) small enough for a macroscopic piece of material to contain a large number of them, allowing us to describe its behavior as an *average* over elements; and (ii) large enough so that deformations on the scale of an element can be described by an elastic strain variable. For a single droplet in a foam, for example, this would not be possible because of its highly nonaffine deformation; in this case, the element size should therefore be at least a few droplet diameters. The size of the elements is chosen as the unit length to avoid cumbersome factors of element volume in the expressions below. We emphasize that the subdivision into mesoscopic elements is merely a conceptual tool for obtaining a suitably coarse-grained description of a SGM. The elements should not be thought of as sharply defined physical entities, but rather as somewhat diffuse ''blobs'' of material. Their size simply represents a coarse-graining length scale whose order of magnitude is fixed by the two requirements (i) and (ii) above.

We denote by l the local shear strain of an element (more generally, the deformation would have to be described by a tensor, but we choose a simple scalar description). To see how l evolves as the system is sheared, consider first the behavior of a foam or dense emulsion. The droplets in an element will initially deform elastically from the local equilibrium configuration, giving rise to a stored elastic energy (due to surface tension, in this example [19]). This continues up to a yield point, characterized by a strain l_y, whereupon the droplets rearrange to new positions in which they are less deformed, thus relaxing stress. The mesoscopic strain l *measured from the nearest equilibrium position* (i.e., the one the element would relax to if there were no external stresses) is then again zero. As the macroscopic strain γ is increased, l therefore executes a ''sawtooth'' kind of motion [36]. Neglecting nonlinearities before yielding, the local shear stress is given by kl, with k an elastic constant; the yield point defines a maximal elastic energy $E=\frac{1}{2}kl_y^2$. The effects of structural disorder are modeled by assuming a *distribution* of such yield energies E, rather than a single value common to all elements. A similar description obviously extends to many others of the soft materials mentioned above.

To make the connection to Bouchaud's glass model, yield events can be viewed as ''hops'' out of a trap (or potential well), and the yield energy E is thereby identified with the trap depth. As before, we assume that yields (hops) are activated by interactions between different elements, resulting in an effective temperature x. The activation barrier is now $E-\frac{1}{2}kl^2$, the difference between the typical yield energy and the elastic energy already stored in the element.

For the behavior of elements in between rearrangements, the simplest assumption is that their strain changes along with the macroscopically imposed strain γ. This means that, yield events apart, the *shear rate* is homogeneous throughout the material; spatial fluctuations of the shear rate are neglected in what can be viewed as a further mean-field approximation. The SGR model therefore applies only to materials that can support macroscopically homogeneous flows (at least in the range of shear rates of practical interest). In fact, we regard this requirement as a working definition of what is meant by a ''soft'' glassy material. A ''hard'' glassy material, on the other hand, might fail by fracture and strong strain localization rather than by homogeneous flow. Whether a link exists between this distinction and the classification of structural glasses into fragile versus strong [33] is not clear to us at present.

While the SGR model assumes a spatially homogeneous *strain rate*, it does admit inhomogeneities in the local *strain* l and *stress* $\sigma=kl$ [37]. These arise because different elements generally yield at different times. To describe the state of the system at a given time, we therefore now need to know the joint probability of finding an element with a yield energy E *and* a local strain l. Within the SGR model [17], this probability evolves in time according to

$$\frac{\partial}{\partial t}P(E,l,t)=-\dot{\gamma}\frac{\partial}{\partial l}P-\Gamma_0\, e^{-[E-(1/2)kl^2]/x}\,P + \Gamma(t)\;\rho(E)\delta(l). \tag{3}$$

The first term on the rhs describes the motion of the elements between rearrangements, with a local strain rate equal to the macroscopic one, $\dot{l}=\dot{\gamma}$. The interaction-activated yielding of elements (which is assumed to be an instantaneous process on the time scales of interest to us) is reflected in the second term. The last term incorporates two assumptions about the properties of an element just after yielding: It is unstrained ($l=0$) and has a new yield energy E randomly chosen from $\rho(E)$, i.e., uncorrelated with its previous one. Finally, the total yielding rate is given by the analog of Eq. (2),

$$\Gamma(t)=\Gamma_0\langle e^{-[E-(1/2)kl^2]/x}\rangle_P = \Gamma_0\int dE\; dl\; P(E,l,t)e^{-[E-(1/2)kl^2]/x}. \tag{4}$$

Equation (3) tells us how the state of the system, described by $P(E,l,t)$, evolves for a given imposed macroscopic strain $\gamma(t)$. What we mainly care about is of course the rheological response, i.e., the macroscopic stress. This is given by the average of the local stresses:

$$\sigma(t)=k\langle l\rangle_P\equiv k\int dE\; dl\; P(E,l,t)l. \tag{5}$$

Equations (3)–(5) define the SGR model, a minimal model for the rheology of SGMs: It incorporates both the ''glassy'' features arising from structural disorder (captured in the dis-

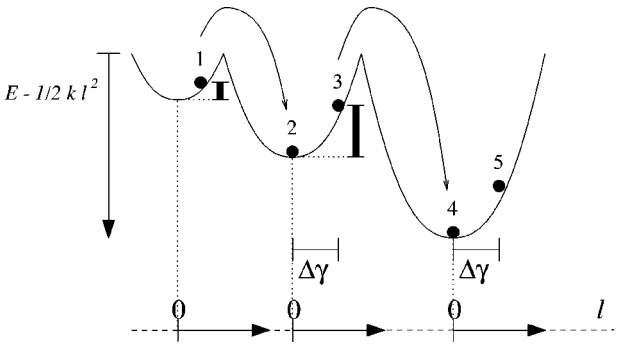

FIG. 2. Potential well picture of the dynamics of the SGR model. Note that the relative horizontal displacement of the quadratic potential wells is arbitrary; each has its own independent zero for the scale of the local strain l. The solid vertical bars indicate the energy dissipated in the ''hops'' (yield events) from 1 to 2 and 3 to 4, respectively.

tribution of yield energies E and local strains l) and the ''softness'': for large macroscopic strains, the material flows because eventually all elements yield. An intuitive picture of the dynamics of the SGR model can be obtained by viewing each element as a ''particle'' moving in a one-dimensional piecewise quadratic potential, with noise-induced hops that become increasingly likely near the edge of a potential well (see Fig. 2). This also shows the hysteresis effects associated with yielding: Once a hop to a new well has taken place, a finite strain reversal is in general needed before a particle will hop back to its old well [38].

Before moving on to the exact solution of the SGR model, we briefly mention some of its limitations. Among the most serious of these is the assumption that the noise temperature x and the attempt frequency Γ_0 are constant parameters of the model. In general, they may be expected to depend on the imposed shear rate $\dot{\gamma}$, for example, or in fact have their own intrinsic time evolution. In particular, it must be borne in mind when interpreting our results below that the effective noise temperature x is not a parameter that we can easily tune from the outside; rather, we expect it to be determined self-consistently by the interactions in the system. We discuss these points in some detail in Sec. VI, where we also speculate on the physical origin of the model parameters x and Γ_0. Within the SGR model, the ''prior'' density of yield energies, $\rho(E)$, is likewise taken to be a constant. This implies the assumption that the structure of the material considered is not drastically altered by an imposed flow, and excludes effects such as shear-induced crystallization.

The SGR model is also essentially a low-frequency model. This is due to our assumption that each element behaves purely elastically until it yields and a rearrangement takes place. In reality, the rheological response of an element will be more complex. After the application of a strain, for example, there may be a fast relaxation of the local stress from its instantaneous value, due to local relaxation processes. In a foam, for example, these might correspond to small shifts of the bubble positions; in the language of mode-coupling theory, they could be described as β relaxations [32,39]. Such local stress relaxation processes are expected to take place much faster than actual yield events, which involve a more drastic reorganization of the structure of the material. For frequencies smaller than the attempt frequency for yielding, $\omega \lesssim \Gamma_0$, they can therefore be neglected. This then implies that the elastic properties that we ascribe to local elements are those that apply once all fast local stress relaxation processes are complete. We have also neglected viscous contributions to the local stress; in foams, for example, these are due to the flow of water and surfactant caused by the deformation of the elements. In the low frequency regime of interest to us, such viscous effects are again insignificant (see, e.g., [11]), whereas at high frequencies the model (3)–(5) would have to be modified appropriately to yield sensible predictions.

Another restriction of the model is the assumption that the elastic constant k is the same for all elements. This may not be appropriate, for example, for strongly polydisperse materials; we plan to investigate the effects of variable k in future work. We have also made the simplifying assumption that an element is always unstrained directly after yielding. Interaction between neighboring elements may, however, frustrate the relaxation to the new equilibrium state; we discuss briefly in Sec. IV C how this feature can be incorporated into the model.

Finally, the treatment of energy dissipation during yield events within the SGR model may also have to be refined. This can be seen by expressing the work done on the system in the following way: We multiply the equation of motion (3) by the elastic energy $\frac{1}{2}kl^2$ of an element and integrate over l and E. Integration by parts of the $\dot{\gamma}$ term then just gives the stress (5), hence

$$\sigma\dot{\gamma} = \frac{d}{dt}\frac{1}{2}\langle kl^2\rangle + \Gamma_0 \frac{1}{2}\langle kl^2 e^{-[E-(1/2)kl^2]/x}\rangle, \qquad (6)$$

where the averages are over $P(E,l,t)$. The left-hand side (lhs) is the rate of energy input into the system. The first term on the rhs, which is a complete time differential, describes the part of this energy that is stored as elastic energy of the elements. The second term, which is always non-negative, is the dissipative part. It is just the average over all elements of their yielding rate times the energy dissipated in a rearrangement, which we read off as $\frac{1}{2}kl^2$. This means that within the model, every rearrangement dissipates exactly the elastic energy stored within the element when it yields (see Fig. 2).

In general, this is not implausible. But it implies that some rearrangements—those of unstrained ($l=0$) elements—have no dissipation associated with them [40]. In reality, however, the local reorganization of a material during *any* yield event would always be expected to dissipate *some* energy. How much might depend, for example, on the height of the activation barrier for yielding, $E-\frac{1}{2}kl^2$. The model in its present form does not capture such effects; in fact, the yield energies E do not feature in the energy balance (6) except through their effect on the yielding rates. This exposes a related limitation of the model: On physical grounds, one would expect that elements with a larger yield energy E may have a more stable configuration with lower total energy (for example, an arrangement of droplets in an emulsion with a lower total surface energy). The average value of E (which increases during aging, for example [12,13]), should then also occur in the energy balance (6). This is not accounted for in the model in its present form.

III. CONSTITUTIVE EQUATION

To simplify the following analysis of the model, we choose appropriate units for energy and time; a convenient choice is such that $x_g=\Gamma_0=1$. From the definition of the glass transition temperature, this implies that the density of yield energies has the form $\rho(E)=\exp\{-E[1+f(E)]\}$ with $f(E)\to 0$ for $E\to\infty$. For our numerical investigations below we use the simplest $\rho(E)$ of this form, which is purely exponential:

$$\rho(E)=\exp(-E). \tag{7}$$

Analytical results, on the other hand, hold for general $\rho(E)$ unless otherwise stated. We eliminate a final parameter from the model by setting $k=1$; this can always be achieved by a rescaling of the stress σ and the strain variables γ and l. With this choice of units, it becomes clear that the SGR model is in fact rather parsimonious: apart from scale factors, its predictions are determined by a single parameter, the effective noise temperature x [41].

Note that in our chosen units, typical yield strains $\sqrt{2E/k}$ are of order one. Experimentally, SGMs generally have yield stresses of at most a few percent (see, e.g., [10,42,43]); the necessary rescaling of our results for strain variables should be borne in mind when comparing to experimental data. For example, a strain rate $\dot{\gamma}=1$ in our units corresponds to $\dot{\gamma}=\overline{l_y}\Gamma_0$ in dimensional units, with $\overline{l_y}=(x_g/k)^{1/2}$ a typical [''*a priori*,'' i.e., sampled from $\rho(E)$] yield strain. For a specific material, the three scale parameters x_g, k, and Γ_0 of the SGR model could be estimated from measurements of a yield strain, a shear modulus, and a viscosity, for example.

The derivation of the exact constitutive equation (CE) for the SGR model is given in Appendix A. For simplicity, we impose the mild restriction that the initial state is completely unstrained, i.e., $\gamma(t=0)=0$ and

$$P(E,l,t=0)=P_0(E)\,\delta(l). \tag{8}$$

Our central result then relates the stress at time t to the strain history $\gamma(t')$ $(0<t'<t)$ by the CE:

$$\sigma(t)=\gamma(t)G_0(Z(t,0)) + \int_0^t dt'\,\Gamma(t')[\gamma(t)-\gamma(t')]G_\rho(Z(t,t')) \tag{9}$$

with the yielding rate $\Gamma(t)$ determined from

$$1=G_0(Z(t,0))+\int_0^t dt'\,\Gamma(t')G_\rho(Z(t,t')). \tag{10}$$

Here the functions

$$G_0(z)=\int dE\; P_0(E)\exp(-ze^{-E/x}),\qquad G_\rho(z)=\int dE\;\rho(E)\exp(-ze^{-E/x}) \tag{11}$$

describe the purely noise induced decay of the stress. This decay is, however, governed not simply by the time interval between a change in macroscopic strain at t' and a stress measurement at t, but by an ''effective time interval'' $z=Z(t,t')$ given by

$$Z(t,t')=\int_{t'}^t dt''\exp\{[\gamma(t'')-\gamma(t')]^2/2x\}. \tag{12}$$

One reads off that $Z(t,t')\geqslant t-t'$; the effective time interval is always *greater* than the actual time interval, and the more so the larger the changes in strain $\gamma(t'')$ from its value at the earlier time t'. This implies a faster decay of the stress, and so $Z(t,t')$ can be said to describe strain-induced yielding (in other words, shear thinning). In fact, a look at Eqs. (9) and (10) confirms that *all* nonlinear effects within the model arise from this dependence of the effective time interval $Z(t,t')$ on the macroscopic strain history $\gamma(t'')$.

The CE (9) and (10) can be most easily understood by viewing the yielding of elements as a birth-death process: Each time an element yields, it ''dies'' and is ''reborn'' with $l=0$. In between such events, its local strain just follows the changes in global strain $\gamma(t)$. If an element was last reborn at time t', its local strain at time t is therefore $l=\gamma(t)-\gamma(t')$. Since we set $k=1$, this is also its contribution to the stress. The first term on the rhs of Eqs. (9) and (10) is the contribution of elements that have ''survived'' from time 0 to t; they do so with the ''survival probability'' $G_0(Z(t,0))$. The second term collects the contribution from all elements that have yielded at least once between time 0 and t, and were last reborn at t'. The number of such elements is proportional to the rate of ''rebirths'' at t', i.e., the yielding rate $\Gamma(t')$, and the corresponding survival probability $G_\rho(Z(t,t'))$. Note that there are two different survival probabilities here, given by G_0 and G_ρ, respectively. The difference arises from the fact that these probabilities are in fact averages over the distribution of yield energies, as expressed by Eq. (11). For elements that have survived from $t'=0$, this distribution is $P_0(E)$, while for elements that have yielded at least once, it is $\rho(E)$.

The glassy features of the SGR model as discussed in Sec. II A are reflected in the CE (9) and (10), in particular in the asymptotic behavior of $G_\rho(z)$. For the simple exponential form (7) of $\rho(E)$, one easily finds that $G_\rho(z)=x!\,z^{-x}$ asymptotically. As shown in Appendix B, the same behavior holds for general $\rho(E)$, in the sense that

$$\lim_{z\to\infty} G_\rho(z)\; z^{x+\epsilon}=\infty,\qquad \lim_{z\to\infty} G_\rho(z)\; z^{x-\epsilon}=0 \tag{13}$$

for any arbitrarily small $\epsilon>0$. We shall refer to this property by saying that $G_\rho(z)$ decays asymptotically as z^{-x} up to ''sub-power-law factors.'' Unless otherwise specified, all power laws referred to in the following hold for general $\rho(E)$, up to such sub-power-law factors.

Consider now the case where strain-induced yielding can be neglected, such that $Z(t,t')=t-t'$. This is always true for sufficiently small strain amplitudes. Below the glass transition $(x<1)$, the time integral $\int_0^t dt'\,G_\rho(t-t')$ of the response function $G_\rho(Z(t,t'))=G_\rho(t-t')$ in Eq. (9) then diverges in the limit $t\to\infty$. Compatible with the intuitive

notion of a glass phase, this means that the system has a very long memory (of the kind that has been described as ''weak long term memory'' [44,45]) and is (weakly [12]) nonergodic. This can lead to rather intricate aging behavior, which we plan to explore in future work. For the purpose of the present paper—with the exception of a brief discussion in Sec. IV B—we focus on situations where the system is ergodic. These include the regime above the glass transition, $x>1$, and the case of steady shear flow for all noise temperatures x (strain-induced yielding here restores ergodicity even for $x<1$). In the former case, a choice needs to be made for the initial distribution of yield energies. We consider the simplest case where this is the equilibrium distribution at the given x:

$$P_0(E)=P_{\rm eq}(E)=\Gamma_{\rm eq}\exp(E/x)\rho(E). \tag{14}$$

Correspondingly, we write $G_0(z)=G_{\rm eq}(z)$. The function $G_\rho(z)$ is then related to the derivative of $G_{\rm eq}(z)$ by

$$G_\rho(z)=-\Gamma_{\rm eq}^{-1}G'_{\rm eq}(z) \tag{15}$$

with a proportionality constant given by the equilibrium yielding rate

$$\Gamma_{\rm eq}^{-1}=\int dE\ \rho(E)\exp(E/x)=\int_0^\infty dz\ G_\rho(z). \tag{16}$$

IV. LINEAR RESPONSE

A. Above the glass transition

The simplest characterization of the rheological behavior of the SGR model is through its linear rheology. This describes the stress response to small shear strain perturbations around the equilibrium state. As such, it is well defined (i.e., time independent) *a priori* only above the glass transition, $x>1$ (see, however, Sec. IV B).

To linear order in the applied strain $\gamma(t)$, the effective time interval $Z(t,t')=t-t'$. In the linear regime, all yield events are therefore purely noise induced rather than strain induced. Correspondingly, the yielding rate as determined from Eq. (10) is simply $\Gamma(t)=\Gamma_{\rm eq}$, as can be confirmed from Eqs. (15) and (16). The expression (9) for the stress can then be simplified to the familiar form

$$\sigma(t)=\int_0^t dt'\,\dot\gamma(t')G_{\rm eq}(t-t'). \tag{17}$$

As expected for an equilibrium situation, the response is time-translation invariant [46], with $G_{\rm eq}(t)$ being the linear stress response to a unit step strain at $t=0$. The dynamic modulus is obtained by Fourier transform,

$$G^*(\omega)=i\omega\int_0^\infty dt\ e^{-i\omega t}G_{\rm eq}(t)=\left\langle\frac{i\omega\tau}{i\omega\tau+1}\right\rangle_{\rm eq}. \tag{18}$$

This an average over Maxwell modes with relaxation times τ. For an element with yield energy E, $\tau=\exp(E/x)$ is just its average lifetime, i.e., the average time between rearrangements. The relaxation time spectrum therefore follows from the equilibrium distribution of energies, $P_{\rm eq}(E)$ $\propto\exp(E/x)\rho(E)$. Because of the exponential tail of $\rho(E)$, it has a power-law tail $P_{\rm eq}(\tau)\sim\tau^{-x}$ (for $\tau\gg1$, up to sub-power-law factors). As x decreases towards the glass transition, this long-time part of the spectrum becomes increasingly dominant and causes anomalous low frequency behavior of the moduli, as shown in Fig. 3:

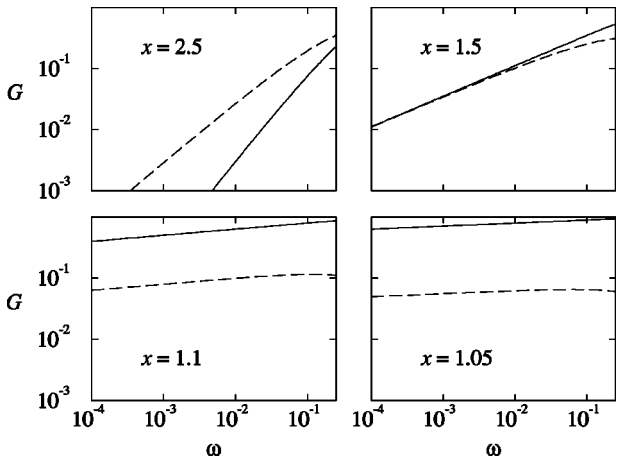

FIG. 3. Linear moduli G' (solid line) and G'' (dashed) vs frequency ω at various noise temperatures x. We only show the behavior in the low frequency regime $\omega\lesssim1$, where the predictions of the SGR model are expected to be physically relevant. The high frequency behavior (predicted as $G'\approx$const, $G''\sim\omega^{-1}$) is not realistic because the model neglects local viscous effects (among others) that can become important in this regime.

$$G'\sim\begin{cases}\omega^2 & \text{for } 3<x,\\ \omega^{x-1} & \text{for } 1<x<3\end{cases}$$
$$G''\sim\begin{cases}\omega & \text{for } 2<x,\\ \omega^{x-1} & \text{for } 1<x<2\,.\end{cases} \tag{19}$$

For $x>3$ the system is Maxwell-like at low frequencies, whereas for $2<x<3$ there is an anomalous power law in the elastic modulus. Most interesting is the regime $1<x<2$, where G' and G'' have constant ratio; both vary as ω^{x-1}. Behavior like this is observed in a number of soft materials [4–7,10]. Moreover, the frequency exponent approaches zero as $x\to1$, resulting in essentially constant values of G'' and G', as reported in dense emulsions, foams, and onion phases [6–8]. Note, however, that the ratio $G''/G'\sim x-1$ becomes small as the glass transition is approached. This increasing dominance of the elastic response G' prefigures the onset of a yield stress for $x<1$ (discussed below). It does not mean, however, that the loss modulus G'' for fixed (small) ω always decreases with x; in fact, it first *increases* strongly as x is lowered and only starts decreasing close to the glass transition (when $x-1\sim|\ln\omega|^{-1}$). The reason for this crossover is that the relaxation time $\tau(\langle E\rangle_{\rm eq})=\exp(\langle E\rangle_{\rm eq}/x)$ corresponding to the mean equilibrium energy $\langle E\rangle_{\rm eq}\sim(x-1)^{-1}$ eventually becomes greater than ω^{-1}.

B. Glass phase

The above linear results only apply above the glass transition ($x>1$), where there is a well defined equilibrium state

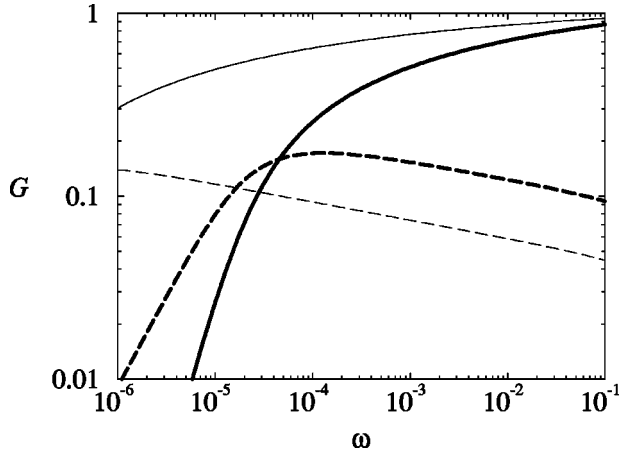

FIG. 4. Linear moduli G' (solid line) and G'' (dashed) vs frequency ω at $x=0.9$ with energy cutoff $E_{\max}=10$ (thick lines) and $E_{\max}=15$ (thin lines). The loss modulus increases as $G''\sim\omega^{x-1}$ as the frequency decreases; at very low frequencies, there is a crossover to Maxwellian behavior.

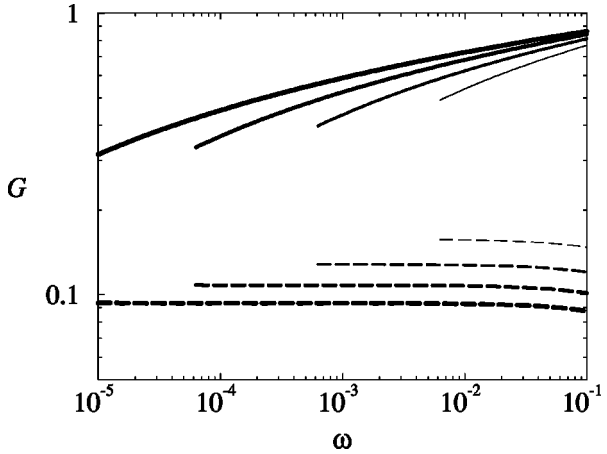

FIG. 5. Age dependence of the dynamic moduli. Shown are G' (solid line) and G'' (dashed) vs frequency ω at $x=1$; lines of increasing thickness correspond to increasing age of the system: $t=10^4$, 10^5, 10^6, 10^7. Frequencies are restricted to the range $\omega t \geqslant 2\pi\times 10$, corresponding to a measurement of $G^*(\omega,t)$ over at least ten oscillation periods. Note the difference in horizontal and vertical scales; both G' and G'' have a very ''flat'' ω dependence.

around which small perturbations can be made. However, if a cutoff $E_{\max}$ on the yield energies is introduced (which is physically reasonable because yield strains cannot be arbitrarily large), an equilibrium state also exists for $x<1$, i.e., below the glass transition. (Strictly speaking, with the cutoff imposed there is no longer a true glass phase; but if the energy cutoff is large enough, its qualitative features are expected to be still present.) One then finds for the low frequency behavior of the linear moduli:

$$G'\approx\text{const}, \quad G''\sim\omega^{x-1}. \tag{20}$$

This applies as long as ω is still large compared to the cutoff frequency, $\omega_{\min}=\exp(-E_{\max}/x)$. In this frequency regime, G'' therefore increases as ω decreases, again in qualitative agreement with some recent experimental observations [7–10]. An example is shown in Fig. 4.

The above results relate to the ''equilibrium'' (pseudo) glass phase. The time to reach this equilibrium state is expected to be of the order of the inverse of the smallest relaxation rate, $\omega_{\min}^{-1}=\exp(E_{\max}/x)$. For large $E_{\max}$, this may be much larger than experimental time scales, and the nonequilibrium behavior will then become relevant instead. We give only a brief discussion here and refer to a future publication [47] for more details. From the CE (9) and (10), it can be deduced quite generally that the stress response to a small oscillatory strain $\gamma(t)=\gamma\ \mathrm{Re}\ \exp(i\omega t)$ switched on at $t=0$ is

$$\sigma(t)=\gamma\ \mathrm{Re}[G^*(\omega,t)e^{i\omega t}]$$

with a time-dependent dynamic modulus

$$G^*(\omega,t)=1-\int_0^t dt' e^{-i\omega(t-t')}\Gamma(t')G_\rho(t-t'). \tag{21}$$

This modulus is physically measurable only for ωt significantly greater than unity, of course, corresponding to a measurement over at least a few periods. Here we consider the case of an initial distribution of yield energies $P_0(E)=\rho(E)$ (hence $G_0\equiv G_\rho$), corresponding to a ''quench'' at $t=0$ from $x\to\infty$ to a finite value of x. We solve Eq. (10) for the yielding rate $\Gamma(t)$ numerically and then evaluate $G^*(\omega,t)$ using Eq. (21). Figure 5 shows the results for a quench to the glass transition ($x=1$). Not unexpectedly, the frequency dependence of the moduli follows the same power laws as in the ''equilibrium'' glass discussed above; the amplitude of these, however, depends on the ''age'' t of the system. For $x<1$, one finds $1-G^*(\omega,t)\sim(\omega t)^{x-1}$ [47]; this time dependence is the same as for the yielding rate $\Gamma(t)$ [13], and is closely related to the aging of the susceptibility in Bouchaud's glass model [12]. The behavior of the loss modulus at the glass transition is particularly noteworthy: Whereas $G''(\omega,t)$ does tend to zero for $t\to\infty$, it does so extremely slowly (as $1/\ln t$), while at the same time exhibiting an almost perfectly ''flat'' ($G''\sim\omega^0$ for small ω) frequency dependence. Where such an ω dependence is observed experimentally it may well, therefore, correspond to a rheological measurement in an out-of-equilibrium aging regime. In order to test this scenario directly, experiments designed to measure a possible age dependence of the linear moduli would be extremely interesting. Such experiments would obviously have to be performed on systems where other sources of aging (such as coalescence in emulsions and foams, evaporation of solvent, etc.) can be excluded; suspensions of microgel beads, hard sphere colloids, or colloid-polymer mixtures might therefore be good candidates.

C. Frustration

As pointed out in Sec. II B, the SGR model in its basic form (3) assumes that after yielding, each element of a SGM relaxes to a completely unstrained state, corresponding to a local strain of $l=0$. This is almost certainly an oversimplification: Frustration arising from interaction of an element with its neighbors will in general prevent it from relaxing completely to its new equilibrium state. This leads to a nonzero local strain l directly after yielding. This effect can be built into the model by replacing the factor $\delta(l)$ in Eq. (3) by

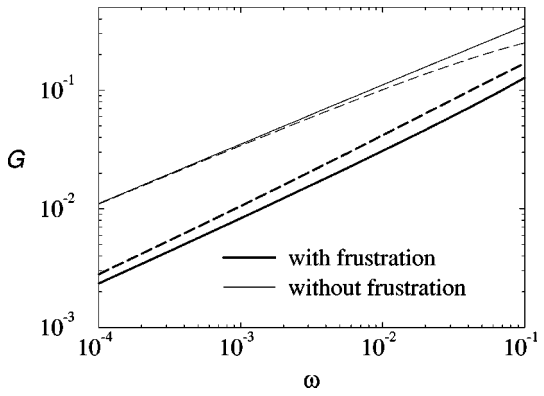

FIG. 6. Effect of frustration. Shown are G' (solid line) and G'' (dashed) vs frequency ω at $x=1.5$; results for uniform frustration (in bold) are compared with the unfrustrated case (thin lines).

a probability distribution $q(l;E)$ of the local strain l after yielding; this distribution will in general also depend on the new yield energy E of the element. We consider here the case of ''uniform frustration,'' where the strain l after yielding has equal probability of taking on any value between $-l_y$ and l_y, with $l_y=(2E)^{1/2}$ being the typical yield strain associated with the new yield energy. Because values of l outside this interval would not make much sense (the element would yield again almost immediately), this scenario can be regarded as maximally frustrated.

An exact CE for such a frustrated scenario can still be derived, but it is rather more cumbersome than Eqs. (9) and (10) due to extra integrations over the strain variable l. The dynamic moduli, however, can still be worked out fairly easily by considering a small perturbation around the steady state of (3) [with $\delta(l)$ replaced by $q(l;E)$]. One finds

$$G^*(\omega)=\left\langle \frac{i\omega\tau}{i\omega\tau+1}+\frac{l^2}{x}\frac{i\omega\tau}{(i\omega\tau+1)^2}\right\rangle_{\rm eq},$$

where the relaxation times $\tau=\exp[(E-\frac{1}{2}l^2)/x]$ are now dependent on both E and l, and the equilibrium distribution over which the average is taken is $P_{\rm eq}(E,l)\propto\exp[(E-\frac{1}{2}l^2)/x]\rho(E)q(l;E)$. For the uniform frustration case, where $q(l;E)=\Theta(E-\frac{1}{2}l^2)/(8E)^{1/2}$, the dynamic moduli are compared with the unfrustrated case in Fig. 6. The main effect of frustration is to add a contribution to the relaxation time spectrum near $\tau\approx1$; this arises from elements that have a strain $l\approx\pm l_y$ after yielding and therefore yield again with a relaxation rate of order unity. Otherwise, however, the main qualitative features of the unfrustrated model are preserved; in particular, it can be shown that the low frequency power-law behavior (19) remains unchanged. We expect that the same will be true for other rheological properties and therefore neglect frustration effects in the following.

V. NONLINEAR RHEOLOGY

Arguably, the *linear* rheological behavior described in the previous section follows inevitably from the existence of a power-law distribution of relaxation times. If we were only interested in the linear regime, it would be simpler just to postulate such a power law. The main attraction of the SGR model is, however, that it also allows nonlinear rheological effects to be studied in detail. It is to these that we now turn.

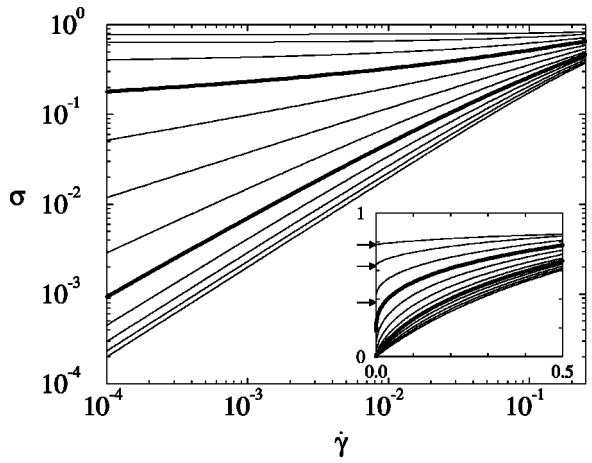

FIG. 7. Shear stress σ vs shear rate $\dot\gamma$, for $x=0.25, 0.5, \ldots, 2.5$ (top to bottom on left); $x=1$ and 2 are shown in bold [71]. The inset shows the behavior on a linear scale, with yield stresses for $x<1$ indicated by arrows.

A. Steady shear flow

1. Flow curves

Steady shear flow ($\dot\gamma=$ const) is one of the simplest probes of nonlinear rheological effects. For the SGR model, the flow curve (shear stress as a function of shear rate) can be calculated either from the long-time limit of the CE (9) and (10), or directly from the steady state solution of the equation of motion (3). Either way, one obtains for the shear stress

$$\sigma(\dot\gamma)=\frac{\int_0^\infty dl\; lG_\rho(Z(l))}{\int_0^\infty dl\; G_\rho(Z(l))} \tag{22}$$

where

$$Z(l)=\frac{1}{\dot\gamma}\int_0^l dl' e^{l'^2/2x}. \tag{23}$$

Equation (22) is just the local strain averaged over its steady state distribution, which is proportional to $G_\rho(Z(l))$ (for $l>0$). The resulting stress can be easily evaluated numerically to give the results in Fig. 7. For large shear rates $\dot\gamma\gtrsim1$, the shear stress σ increases very slowly for all x [$\sigma\sim(x\ln\dot\gamma)^{1/2}$], corresponding to strong shear thinning. More interesting (and more physically relevant [48]) is the small $\dot\gamma$ behavior, where we find three regimes:

(i) For $x>2$, the system is Newtonian, $\sigma=\eta\dot\gamma$, for $\dot\gamma\to0$. The viscosity can be derived by noting that in this regime, the size of the local strains l that contribute significantly to σ is proportional to $\dot\gamma$. For $\dot\gamma\to0$, this decreases to zero, and we can approximate $Z(l)=l/\dot\gamma$, giving

$$\eta=\frac{\sigma}{\dot\gamma}=\frac{\int_0^\infty dt\ tG_\rho(t)}{\int_0^\infty dt\ G_\rho(t)}$$

$$=\Gamma_{\rm eq}\int dE\ \rho(E)e^{2E/x}=\langle e^{E/x}\rangle_{\rm eq}=\langle\tau\rangle_{\rm eq}.$$

The viscosity is therefore simply the average of the relaxation time $\tau=\exp(E/x)$ over the equilibrium distribution of energies, $P_{\rm eq}(E)=\Gamma_{\rm eq}\exp(E/x)\rho(E)$. From the form $\eta\propto\langle\exp(2E/x)\rangle_\rho$ one sees that it diverges at $x=2$, i.e., at *twice* the glass transition temperature. The existence of several characteristic temperatures in the SGR model is not surprising; in fact, Bouchaud's original glass model already has this property [13] (which has also been discussed in more general contexts, see e.g., [49]).

(ii) The divergence of the viscosity for $x\to2$ signals the onset of a new flow regime: for $1<x<2$ one finds power-law fluid rather than Newtonian behavior. The power-law exponent can be derived as follows: The steady shear stress (22) is the ratio of the integrals

$$I_n(\dot\gamma)=\int_0^\infty dl\ l^nG_\rho(Z(l))$$

for $n=1$ and $n=0$. By techniques very similar to those used in Appendix B, one derives that in the small $\dot\gamma$ limit, I_n scales as $\dot\gamma^{n+1}$ for $x>n+1$; for lower x, there is an additional contribution scaling as $\dot\gamma^x$ up to sub-power-law factors (see Appendix C). The dominant contribution to σ for small $\dot\gamma$ in the regime $1<x<2$ therefore scales as $\sigma\sim\dot\gamma^{x-1}$, again up to sub-power-law factors. The power-law fluid exponent thus decreases linearly, from a value of one for $x=2$ to zero at the glass transition $x=1$.

(iii) For $x<1$, the system shows a yield stress: $\sigma(\dot\gamma\to0)=\sigma_{\rm y}>0$. This can again be understood from the scaling of I_1 and I_0: the dominant small $\dot\gamma$ contributions to both scale as $\dot\gamma^x$ for $x<1$, giving a finite ratio $\sigma_y=I_1/I_0$ in the limit $\dot\gamma\to0$. For general $\rho(E)$ there are subtleties due to sub-power-law corrections here, which are discussed in Appendix C. Here we focus on the simplest case (7) of exponential $\rho(E)$, where such corrections are absent. Using the scaling of I_1 and I_0, we can then write the shear stress for small $\dot\gamma$ as

$$\sigma=\frac{O(\dot\gamma^x)+O(\dot\gamma^2)}{O(\dot\gamma^x)+O(\dot\gamma^1)}=\sigma_{\rm y}+O(\dot\gamma^{1-x}).\qquad(24)$$

Beyond yield, the stress therefore again increases as a power law of the shear rate, $\sigma-\sigma_{\rm y}\propto\dot\gamma^{1-x}$. For exponential $\rho(E)$, the yield stress itself can be calculated explicitly: In order to have $\sigma_y>0$, the values of l that contribute to the shear stress (22) must remain finite for $\dot\gamma\to0$. But then for any fixed l, $Z(l)\to\infty$. We can therefore use the asymptotic form $G_\rho(z)=x!z^{-x}$ in Eq. (22), giving

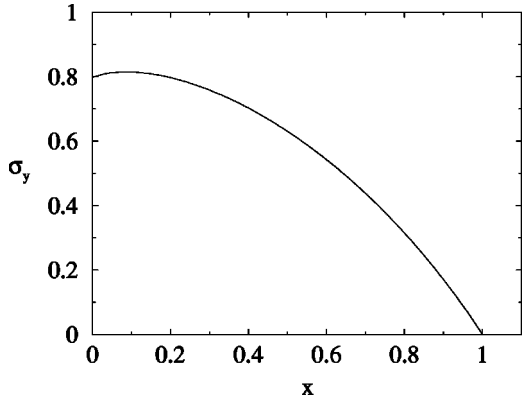

FIG. 8. Yield stress σ_y as a function of x.

$$\sigma_{\rm y}=\frac{\int_0^\infty dl\ l[Z(l)]^{-x}}{\int_0^\infty dl[Z(l)]^{-x}}.\qquad(25)$$

The factor $\dot\gamma^x$ [from the definition (23) of $Z(l)$] in the numerator and denominator has canceled, making the result independent of $\dot\gamma$ as required. Figure 8 shows the resulting yield stress as a function of x; it has a linear onset near the glass transition, $\sigma_{\rm y}\sim1-x$.

To summarize, the behavior of the SGR model in regimes (ii) and (iii) matches respectively the power-law fluid [1–3] and Herschel-Bulkeley [1,2] scenarios as used to fit the nonlinear rheology of pastes, emulsions, slurries, etc. In regime (ii), the power-law exponent is simply $x-1$, x being the effective (noise) temperature; in regime (iii) and for exponential $\rho(E)$, it is $1-x$ (see Appendix C for a discussion of the general case). Numerical data for the effective exponent $d\ln(\sigma-\sigma_{\rm y})/d\ln\dot\gamma$ in Fig. 9 are compatible with this, although the exponent only approaches its limiting value very slowly as $\dot\gamma\to0$ for x near the boundaries of the power-law regime, $x=1$ and 2.

A natural question to ask is of course how the existence of a yield stress in the glass phase affects the linear moduli, i.e., the response to small strains. This is a highly nontrivial issue due to the nonergodicity of the glass phase and the corre-

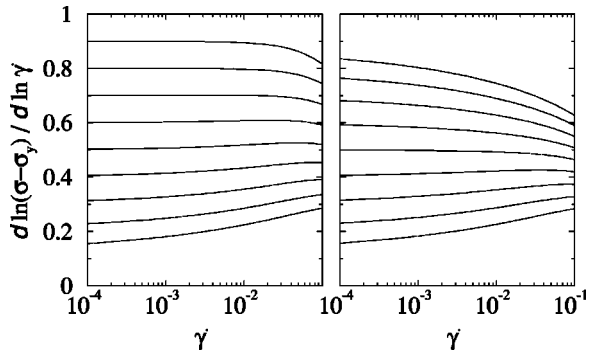

FIG. 9. Effective power-law exponent $d\ln(\sigma-\sigma_{\rm y})/d\ln\dot\gamma$ vs $\dot\gamma$ in the glass phase (left, yield stress $\sigma_{\rm y}>0$, $x=0.1, 0.2, \ldots, 0.9$ from top to bottom) and in the power-law fluid regime (right, $\sigma_y=0$, $x=1.1, 1.2, \ldots, 1.9$ from bottom to top).

sponding aging behavior. In particular, the answer will depend to a significant degree on the strain history of the material. We therefore leave this point for future, more detailed study [47].

2. Flow interrupts aging

We saw above that there is a steady state regime for *any value of x* in the presence of steady shear flow. On the other hand, the discussion in Secs. III and IV B showed that in the absence of flow, the system has no steady state in the glass phase ($x<1$) and instead exhibits aging behavior. The difference between the two cases can be seen more clearly by considering the distribution of yield energies, $P(E)$. Without flow, one obtains a Boltzmann distribution $P(E) \propto \rho(E)\exp(E/x)$ up to (for $x<1$) a ''soft'' cutoff that shifts to higher and higher energies as the system ages [13]. This cutoff, and hence the most long-lived traps visited (which have a lifetime comparable to the age of the system), dominate the aging behavior [12]. In the presence of flow, on the other hand, there is a finite steady state value for this cutoff; one finds

$$P(E)\propto\rho(E)e^{E/x} \quad \text{for } E\ll x\ln(\dot\gamma^{-1}x^{1/2}), \qquad (26)$$

$$P(E)\propto\rho(E)E^{1/2} \quad \text{for } E\gg x\ln(\dot\gamma^{-1}x^{1/2})$$

(only the second regime exists for $\dot\gamma\gtrsim x^{1/2}$). The existence of these two regimes can be explained as follows: Assume the yielding of an element is noise-induced. Its typical lifetime is then $\exp(E/x)$, during which it is strained by $\dot\gamma\exp(E/x)$. The assumption of noise-induced yielding is self-consistent if this amount of strain does not significantly enhance the probability of yielding, i.e., if $[\dot\gamma\exp(E/x)]^2/x\ll 1$. This is the low E regime in Eq. (26), which gives a Boltzmann form for the yield energy distribution as expected for noise-induced yielding. In the opposite regime, yielding is primarily strain induced, and the time for an element to yield is of the order of $l_y/\dot\gamma=(2E)^{1/2}/\dot\gamma$ [rather than $\exp(E/x)$]. Intuitively, we see that flow prevents elements from getting stuck in progressively deeper traps and so truncates the aging process after a finite time. We can therefore say that ''flow interrupts aging'' [14].

3. Cox-Merz rule

A popular way of rationalizing flow curves is by relating them to the linear rheology via the heuristic Cox-Merz rule [50]. This rule equates the ''dynamic viscosity'' $\eta^*(\omega)=|G^*(\omega)|/\omega$ with the steady shear viscosity $\eta(\dot\gamma)=\sigma(\dot\gamma)/\dot\gamma$ when evaluated at $\dot\gamma=\omega$. The ratio $\omega\eta(\dot\gamma=\omega)/|G^*(\omega)|$ is therefore equal to unity if the Cox-Merz rule is obeyed perfectly. Using our previous results, we can easily verify whether this is the case in the SGR model. From Fig. 10, we see that in the Newtonian regime $x>2$, the Cox-Merz rule is obeyed reasonably well for frequencies $\omega \lesssim 1$; for $\omega\to 0$, it holds exactly as expected [recall that $\eta(\dot\gamma)=\langle\tau\rangle$, while from Eq. (19), $G^*(\omega\to 0)=i\omega\langle\tau\rangle$]. In the power-law fluid regime $1<x<2$, on the other hand, the Cox-Merz rule is seen to be less reliable and is not obeyed exactly even in the zero frequency limit. At the glass transition ($x\to 1$), it fails rather dramatically: In this limit, $|G^*(\omega)|=1$ and so the Cox-Merz rule predicts a shear rate independent shear stress $\sigma(\dot\gamma)=\dot\gamma\eta(\dot\gamma)=1$, whereas in fact $\sigma(\dot\gamma)$ decreases to zero for $\dot\gamma\to 0$.

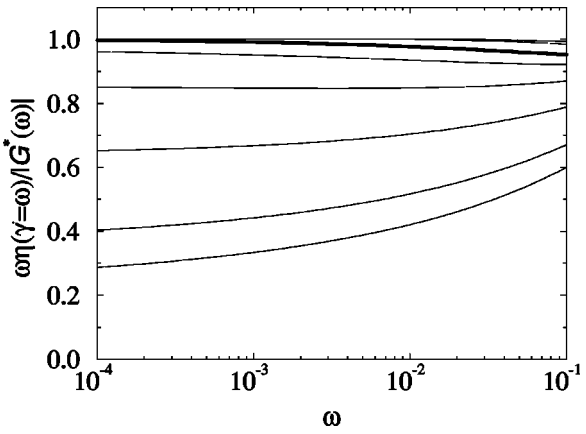

FIG. 10. Cox-Merz ratio $\omega\eta(\dot\gamma=\omega)/|G^*(\omega)|$ as a function of ω for noise temperatures $x=1$, 1.2, . . . , 1.8, 2 (bold), 2.5, 3 (bottom to top).

4. Dissipation under steady shear

Finally, in conclusion of this section on steady shear flow, we calculate the distribution of energies dissipated in yield events. This distribution may provide a useful link to computer simulations of steady shear flow of foams, for example, where it is often easy to monitor discontinuous drops in the total energy of the system and determine their distribution [23]. The correspondence is, however, not exact. Our mean-field model treats all yield events as uncorrelated with each other, in both time and space. In reality, such correlations will of course exist. In fact, several events may occur simultaneously, at least within the time resolution of a simulation or experiment. The observed drop in total energy would then have to be decomposed into the contributions from the individual events to allow a direct comparison with our model. This is only possible if the events are sufficiently localized (spatially) to make such a decomposition meaningful. In foams and emulsions, there is evidence that this may indeed be the case [20,23,42,51–55].

We earlier derived the energy balance equation (6) and deduced from it that, within the model, each yield event dissipates the elastic energy $\Delta E=\frac{1}{2}l^2$ stored in the element just prior to yielding. The probability of observing a yield event with energy dissipation ΔE is therefore given by

$$P(\Delta E)=\frac{1}{\Gamma}\int dE\ dl\ P(E,l)e^{-[(E-\frac{1}{2}l^2])/x}\delta(\Delta E-\tfrac{1}{2}l^2).$$

The steady state distribution $P(E,l)$ of yield energies and local strains for a given shear rate $\dot\gamma$ and noise temperature x can easily be deduced from Eq. (3). After some algebra, the result can be put into the simple form

$$P(\Delta E)d\Delta\ \ E=-\frac{\partial}{\partial l}G_\rho(Z(l))dl.$$

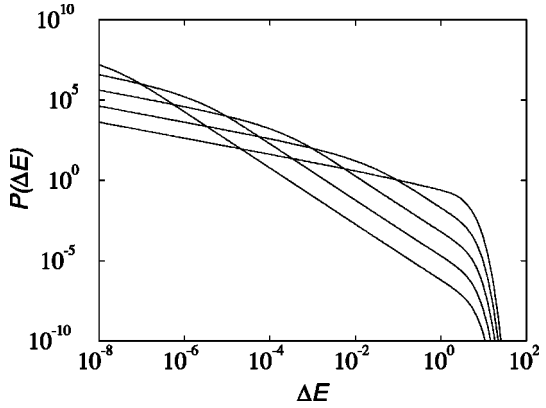

FIG. 11. Distribution $P(\Delta E)$ of energies ΔE dissipated in yield events under steady flow, for $x=1.5$ and $\dot{\gamma}=10^{-4}$, 10^{-3}, ..., 1 (bottom to top at $\Delta E=1$)

Figure 11 shows the resulting $P(\Delta E)$ for exponential $\rho(E)$. Larger shear rates $\dot{\gamma}$ are seen to lead to an increasing dominance of ''large'' yield events (which dissipate a lot of energy). This is intuitively reasonable: the larger $\dot{\gamma}$, the larger the typical strains of elements when they yield. The functional dependence of $P(\Delta E)$ on ΔE is surprisingly simple. An initial power-law decay $P(\Delta E)\sim\Delta E^{-1/2}$ crosses over for $\Delta E\approx\dot{\gamma}^2$ into a second power-law regime $P(\Delta E)\sim\Delta E^{-1-x/2}$. This is cut off exponentially for values of ΔE around unity [56]. The exponential tail for very large dissipated energies is $P(\Delta E)\sim\exp(-\Delta E)$ independently of x. This asymptotic behavior is the same as for the prior density of yield energies, $\rho(E)\sim\exp(-E)$; measurements of $P(\Delta E)$ for large ΔE could therefore yield valuable information on $\rho(E)$.

These results for $P(\Delta E)$ also help one to understand the small $\dot{\gamma}$ scaling of the energy dissipation rate $\sigma\dot{\gamma}=\Gamma\langle\Delta E\rangle$. From the results of Sec. V A, we know that this is $\dot{\gamma}^2$ in the Newtonian regime $x>2$, $\dot{\gamma}^x$ in the power-law fluid range $1<x<2$, and $\dot{\gamma}$ in the yield stress regime $x<1$. (The limit $\dot{\gamma}\to 0$ is always understood here and in the following.) The form of $P(\Delta E)$ suggests decomposing the dissipation into its contributions from ''small'' $[\Delta E=O(\dot{\gamma}^2)]$ and ''large'' $[\Delta E=O(1)]$ dissipation events. Each of these two classes makes a contribution to $\sigma\dot{\gamma}$ that is the fraction of elements in the class, times the average yielding rate in the class, times the average energy dissipated. Hence, in obvious notation,

$$\sigma\dot{\gamma}=P_s\Gamma_s\Delta E_s+P_l\Gamma_l\Delta E_l\,.$$

One then easily confirms the following scalings. The average *dissipated energies* are obviously given by $\Delta E_s=O(\dot{\gamma}^2)$ and $\Delta E_l=O(1)$. The average *yielding rate* for the small, noise induced events is independent of shear rate, $\Gamma_s=O(\dot{\gamma}^0)$; while for the large, shear induced events it is $\Gamma_l=O(\dot{\gamma})$. Finally, for the *fractions* of small and large elements, one finds that *above* the glass transition, almost all elements have small strains $l=O(\dot{\gamma})$, corresponding to $\Delta E=O(\dot{\gamma}^2)$; hence $P_s=O(1)$. Large strains, on the other hand, occur with a probability $P_l=O(\dot{\gamma}^{x-1})$ which becomes vanishingly small for small shear rates. *Below* the glass transition, the situation is reversed: $P_l=O(1)$, while $P_s=O(\dot{\gamma}^{1-x})$. Putting everything together, one has the following:

(i) In the Newtonian regime $(x>2)$, dissipation is dominated by small, noise-induced events, and is therefore of $O(\dot{\gamma}^2)$.

(ii) In the power-law fluid range $(1<x<2)$, a vanishingly small number of elements has large strains, but these dominate the dissipation $\sigma\dot{\gamma}=P_l\Gamma_l\Delta E_l=O(\dot{\gamma}^{x-1})O(\dot{\gamma})=O(\dot{\gamma}^x)$. As the glass transition is approached, the fraction of large elements and hence the dissipation increases.

(iii) In the yield stress regime, most elements have large strains, giving a dissipation rate $\sigma\dot{\gamma}=O(\dot{\gamma})$ that simply scales with the shear rate.

With the same approach, one can also analyze the total *yielding rate* $\Gamma=P_s\Gamma_s+P_l\Gamma_l$. Small events always dominate, and Γ therefore scales with $\dot{\gamma}$ in the same way as P_s. This is true even in the non-Newtonian flow regimes $(x<2)$, where the contribution of these elements to the total *dissipation rate* is negligible.

The distribution of total energy drops $\Delta E_{\rm tot}$ due to rearrangements has been monitored in recent simulations of steady shear flow of two-dimensional foam, based on a ''soft-sphere model'' [22,23]. It was found to exhibit a power law $P(\Delta E_{\rm tot})\sim\Delta E_{\rm tot}^{-\nu}$ with an exponent $\nu\approx 0.7$, with an exponential cutoff for large energy drops. More recent simulations using the same model suggest that, when $\Delta E_{\rm tot}$ is normalized by the average elastic energy per foam bubble, the form of $P(\Delta E_{\rm tot})$ is largely insensitive to variations in shear rate $\dot{\gamma}$. Decreasing the gas volume fraction ϕ moves the (normalized) cutoff to larger energies, suggesting a possible divergence near the rigidity loss transition at $\phi\approx 0.64$ [57]. Simulations using a ''vertex model,'' on the other hand, gave $P(\Delta E_{\rm tot})\sim\Delta E_{\rm tot}^{-3/2}$ with no system-size–independent cutoff for large $\Delta E_{\rm tot}$ [21]. It is unclear how these results can be reconciled; neither, however, is fully compatible with the predictions of the SGR model for $P(\Delta E)$. At this point, we do not know whether this disagreement is due to the difference between ΔE (dissipation in a single yield event) and $\Delta E_{\rm tot}$ (total dissipation in a number of simultaneous yield events), or whether it points to a more fundamental shortcoming of the SGR model such as neglect of spatial or temporal correlations.

B. Shear startup

If a shear flow is started up at $t=0$, such that $\gamma(t)=\dot{\gamma}t$ for $t\geqslant 0$, then $\sigma(\dot{\gamma})$ as given by the flow curve is the asymptotic, steady state value of the stress for $t\to\infty$. We now consider the transient behavior $\sigma(t)$ for finite t. This depends on the initial state of the system at $t=0$; here we consider only the case where this initial state is the equilibrium state (14) at the given value of x. This restricts our discussion to the regime above the glass transition, $x>1$, where such an equilibrium state exists [58]. Solving the CE (9) and (10) numerically, we can find the stress σ as a function of time t or, alternatively, strain γ. Figure 12 shows exemplary results. The initial behavior under shear startup is found to be elastic in all cases, $\sigma=\gamma$. [This can in fact be deduced directly by ex-

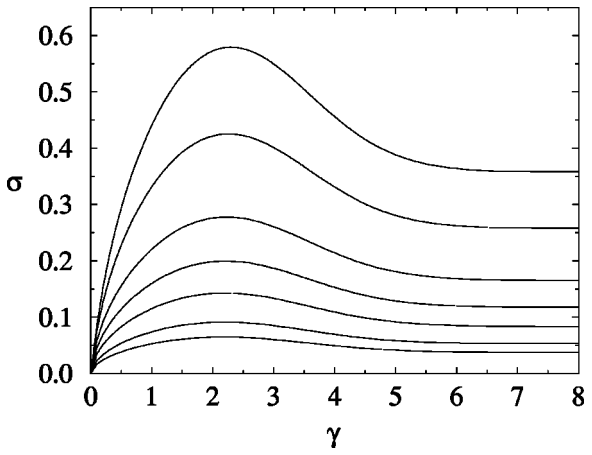

FIG. 12. Stress σ vs strain γ for shear startup at effective temperature $x=1.5$. The shear rate $\dot{\gamma}=0.001$, 0.002, 0.005, 0.01, 0.02, 0.05, 0.1 increases from bottom to top.

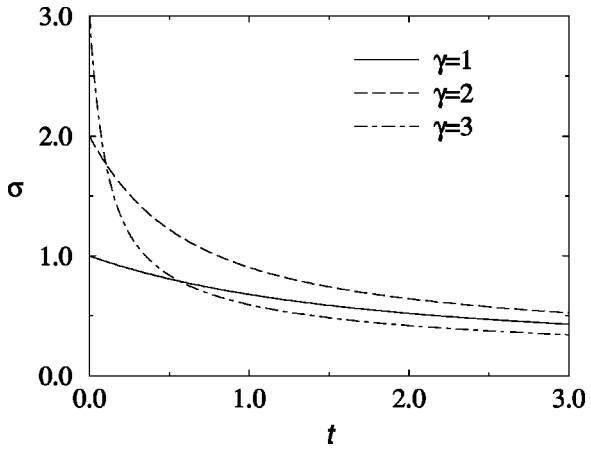

FIG. 13. Stress response to step strains of amplitude $\gamma=1$, 2, 3, at noise temperature $x=1.5$.

panding Eq. (9) to first order in t and noting that $G_0(Z(t,0))=1+O(t)$ while the contribution from the integral is of $O(t^2)$.] Asymptotically, on the other hand, the stress approaches the steady-state (flow curve) value $\sigma(\dot{\gamma})$. However, the model predicts that it does not necessarily do so in a monotonic way. Instead, the stress can ''overshoot''; within the model, this effect is most pronounced near the glass transition ($x\approx 1$). Such overshoot effects have been observed experimentally in, for example, foam flow [6]. The tendency towards large overshoots for $x\to 1$ agrees with our results for the linear moduli and flow curves: As the glass transition is approached, the behavior of the system becomes predominantly elastic; the stress can therefore increase to larger values in shear startup before the material (as a whole) yields and starts to flow.

C. Large step strains

As a further probe of the nonlinear rheological behavior predicted by the SGR model, we now consider large (single and double) step strains. Again, we do not discuss aging effects here and therefore limit ourselves to the regime $x>1$ with the equilibrium initial condition (14).

The case of a single step strain [$\gamma(t)=\gamma\Theta(t)$, with $\Theta(t)=1$ for $t>0$ and zero otherwise] is particularly simple. The integral over t' in the CE (9) is then identically zero, giving a stress response of

$$\sigma(t)=\gamma G_0(Z(t,0))=\gamma G_{\rm eq}(e^{\gamma^2/2x}t). \tag{27}$$

Comparing with the response (17) in the linear regime, the effect of nonlinearity is to speed up all relaxation processes by a factor $\exp(\gamma^2/2x)$. It is easy to see why this is the case. Because we are starting from an unstrained equilibrium configuration, each element initially has $l=0$ and a yielding rate $\exp(-E/x)$. Directly after the strain is applied, it therefore has local strain $l=\gamma$; this increases its relaxation rate to $\exp[-(E-\frac{1}{2}\gamma^2)/x]$, i.e., by the same factor $\exp(\gamma^2/2x)$ for all elements. Figure 13 illustrates this effect of strain nonlinearity; note that the stress for large step strains can decay to small values faster than for small strains, due to the strain-induced speedup of all relaxation processes.

Interestingly, the *instantaneous* response is always elastic and not affected by nonlinear effects: $\sigma(t=0^+)=\gamma$ for all γ. It is easily shown from the CE (9) and (10) that this is a general feature of the SGR model; whenever the macroscopic strain $\gamma(t)$ changes discontinuously by $\Delta\gamma$, the stress $\sigma(t)$ changes by the same amount. We also note that the stress response (27) cannot be factorized into time and strain dependence. However, for the particular case of exponential $\rho(E)$ and long times $\exp(\gamma^2/2x)t\gg 1$, such a factorization does exist due to the asymptotic behavior of $G_{\rm eq}$, $G_{\rm eq}(z)\sim z^{1-x}$. [This follows from $G_\rho(z)\sim z^{-x}$ and Eq. (15).] One then has

$$\sigma(t)\sim\gamma h(\gamma)G_{\rm eq}(t),\quad h(\gamma)=\exp[-\tfrac{1}{2}(1-x^{-1})\gamma^2].$$

The product $\gamma h(\gamma)$ tends to zero as γ increases, corresponding to a pronounced shear-thinning effect.

By applying two (large) step strains in sequence, one can further probe the nonlinear response of the SGR model. Let γ_1 and γ_2 be the amplitudes of the two strains. If the first strain is applied at $t=0$ and the second one at $t=\Delta t$, then $\gamma(t)=\gamma_1\Theta(t)+\gamma_2\Theta(t-\Delta t)$. It is straightforward to solve the CE (9) and (10) numerically for $t>\Delta t$. Figure 14 exemplifies the results for the two cases where the strains are either equal or of equal magnitude but opposite sign. In the first case, and more generally when $\gamma_1\gamma_2>0$, the second step strain speeds up the stress relaxation (by a factor $\exp\{[(\gamma_1+\gamma_2)^2-\gamma_1^2]/2x\}$ for small Δt). Therefore, even though the stress is increased momentarily when the second strain is applied, it can actually relax back to zero more quickly than in the absence of this strain. In the second case ($\gamma_1\gamma_2<0$), the second step strain can to some degree reverse the speedup from the first step strain. A particularly simple form of the resulting stress response is obtained for $\gamma_1=-\gamma_2=\gamma$ and small Δt:

$$\sigma(t>\Delta t)=-\gamma[1-G_{\rm eq}(e^{\gamma^2/2x}\Delta t)]G_\rho(e^{\gamma^2/2x}(t-\Delta t)).$$

This can be understood by noting that the stress for $t>\Delta t$ is due entirely to elements that have yielded between the application of the first and the second strain; all other elements have simply followed the two changes of macroscopic strain and are therefore back to their unstrained state $l=0$ after the

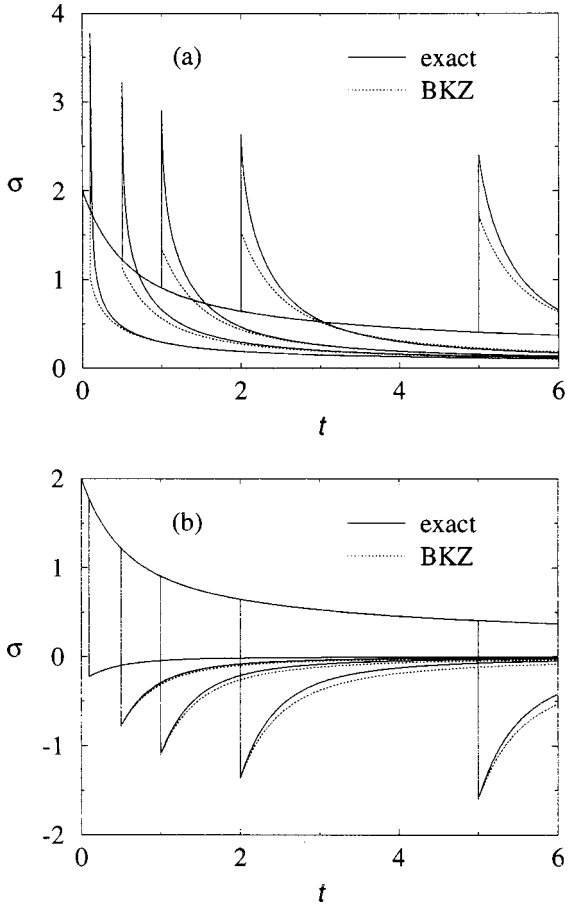

FIG. 14. Stress response to two large step strains of (a) equal ($\gamma_1=\gamma_2=2$) and (b) opposite ($\gamma_1=-\gamma_2=2$) sign, applied at times $t=0$ and $t=\Delta t=0.1$, 0.5, 1, 2, 5, respectively. Noise temperature $x=1.5$.

second strain. The factor in squared brackets just gives the fraction of such elements. The time dependence of the ensuing stress relaxation is determined by G_ρ rather than $G_{\rm eq}$ because elements that have yielded were ''reborn'' with yield energies sampled from $\rho(E)$. These elements—which have ''forgotten'' about the first step strain—also receive a speedup of their relaxation by the second strain.

The above results can be compared to the predictions of the empirical BKZ (Bernstein, Kearseley, Zapas) equation [59]. This relation approximates the stress response to an arbitrary strain history in terms of the response $\sigma(t)=\phi(t,\gamma)$ to a step strain of size γ at time $t=0$:

$$\sigma_{\rm BKZ}(t)=\int_{-\infty}^{t} dt' \frac{\partial}{\partial t'}\phi(t-t',\gamma)\big|_{\gamma=\gamma(t)-\gamma(t')}.$$

For two step strains, this gives, for $t>\Delta t$,

$$\sigma_{\rm BKZ}(t)=\phi(t,\gamma_1+\gamma_2)-\phi(t,\gamma_2)+\phi(t-\Delta t,\gamma_2). \quad (28)$$

In our case, $\phi(t,\gamma)$ is given by Eq. (27), and the BKZ prediction is plotted in Fig. 14 along with the exact results. One finds that for the SGR model, the BKZ equation is at best approximate, at worst qualitatively wrong. This is most easily seen in the size of the stress jump at $t=\Delta t$; the BKZ equation predicts

$$\phi(0^+,\gamma_2)+[\phi(\Delta t,\gamma_1+\gamma_2)-\phi(\Delta t,\gamma_1)-\phi(\Delta t,\gamma_2)]. \quad (29)$$

Because $\phi(0^+,\gamma)=\gamma$ within the SGR model, the term in square brackets is the deviation from the exact result of γ_2. For $\gamma_1=-\gamma_2$, the BKZ prediction for the stress jump is exact because $\phi(t,\gamma)=-\phi(t,-\gamma)$; in this case [Fig. 14(b)], it also works reasonably well for the subsequent stress relaxation. In the general case, however, it is unreliable; Fig. 14(a) shows that it can in fact even predict the wrong sign for the stress jump.

Finally, we note that a failure of the BKZ equation has also been observed in double step strain experiments on polymeric liquids [60]. There, however, the most pronounced deviations occur for successive step strains of opposite sign rather than, as in the SGR model, for strains of the same sign. This can be understood on the basis of the different kinds of nonlinearities in the two cases. Roughly speaking, in the polymer case the BKZ equation fails because it neglects memory of the shape of the tube in which a given polymer molecule reptates [60,61]. Such memory effects are strongest for *strain reversal*, which can bring the tube back to a conformation close to its original shape. In the SGR model, on the other hand, the BKZ equation fails because it does not adequately represent the effects of the strain history on the stress relaxation rates in the material. Such effects are strongest when an applied strain compounds an earlier speedup of relaxation processes, i.e., for double step strains of the *same sign*.

D. Large oscillatory strains

1. Dynamic moduli

As a final example of nonlinear rheological behavior, we consider the case of large oscillatory strains. We remind the reader at this point that we have chosen units in which typical local yield strains are of order unity (see Sec. III). To transform to experimentally relevant quantities, all strain values have to be multiplied by a typical yield strain $\overline{l_y}$ of the SGM under consideration. A strain $\gamma=1$ in our units therefore corresponds to a real strain of generally at most a few percent.

We consider only the ergodic regime $x>1$; we also ignore transient behavior caused by startup of the oscillatory strain. In the steady state, we can write the stress response to an oscillatory strain $\gamma(t)=\gamma\,{\rm Re}\,e^{i\omega t}$ as

$$\sigma(t)=\gamma\,{\rm Re}[G^*(\omega,\gamma)e^{i\omega t}]+\Delta\sigma(t), \quad (30)$$

where $\Delta\sigma(t)$ contains the contributions from all higher harmonics. This defines an amplitude dependent dynamic modulus $G^*(\omega,\gamma)$; the relative root-mean-square size of the stress contributions from higher harmonics is measured by the residual r, defined by

$$r^2=\frac{\int dt\ [\Delta\sigma^2(t)]^2}{\int dt\ \sigma^2(t)}. \quad (31)$$

The determination of G^* and r from the CE (9) and (10) presents no conceptual difficulties, but is somewhat non-

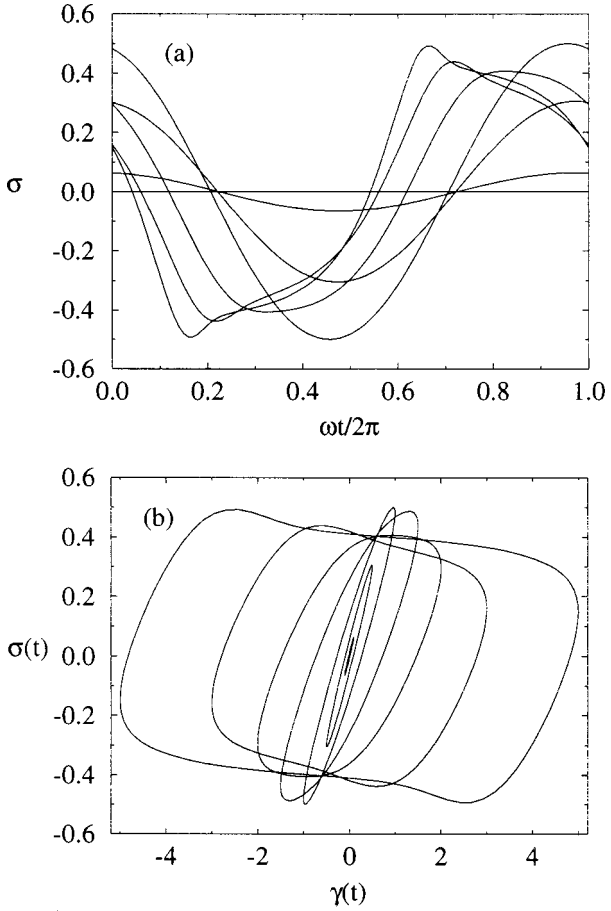

FIG. 15. (a) Stress response $\sigma(t)$ for oscillatory strain $\gamma(t) = \gamma\cos(\omega t)$, for frequency $\omega = 0.01$ and effective temperature $x = 1.1$. Initially, the response is almost perfectly elastic; as the strain amplitude increases (curves are shown for $\gamma = 0.1$, 0.5, 1, 2, 3, 5), the zero crossings of $\sigma(t)$ move to the left, corresponding to progressively liquidlike behavior (strain lagging behind stress). (b) Parametric plots of stress $\sigma(t)$ vs strain $\gamma(t)$, for same parameter values as in (a); $\gamma = 1.5$ is also shown.

trivial numerically (see Appendix D for details). The solution yields in fact not just G^* and r, but the whole ''wave form'' of the stress response $\sigma(t)$. Figure 15(a) shows how the response becomes more and more nonsinusoidal as the strain amplitude is increased. The stress amplitude first increases linearly with γ, then drops slightly as the system crosses over from elastic to liquidlike behavior, and finally rises again slowly as the typical shear rate $\gamma\omega$ of the (now essentially liquefied) material increases. Plotting $\gamma(t)$ and $\sigma(t)$ in a parametric stress-strain plot [Fig. 15(b)], one finds a hysteresis loop for large amplitudes, with stress overshoots near the points where the strain rate reverses its sign.

Consider now the resulting nonlinear modulus G^*. Figure 16 shows an example of a ''strain sweep'': The moduli G' and G'' and the residual r are plotted as a function of strain amplitude for different frequencies ω. The amplitude dependence of G'' is particularly noteworthy: As γ increases, G'' first increases, but then passes through a maximum and subsequently decreases again. This is in qualitative agreement with recent measurements of nonlinear dynamic moduli in, for example, dense emulsions and colloidal glasses [7,10,62,63]. The maximum in G'' is most pronounced near

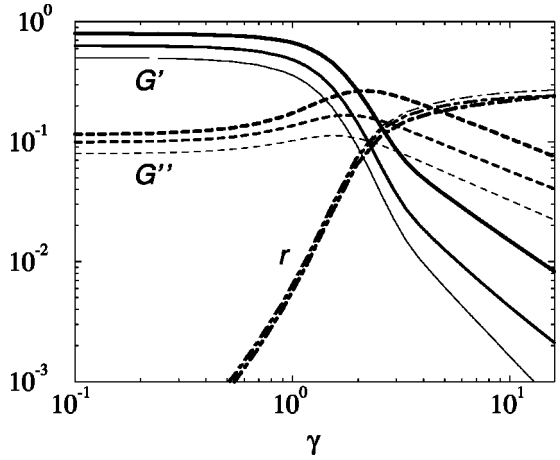

FIG. 16. Strain sweep: Nonlinear moduli G', G'' and residual r as a function of strain amplitude γ. Noise temperature $x = 1.1$; lines of increasing thickness correspond to $\omega = 0.001$, 0.01, 0.1. Recall that γ is rescaled by a typical local yield strain; $\gamma = 1$ therefore corresponds to a real strain of at most a few percent.

the glass transition $x = 1$; for higher noise temperatures, it decreases and disappears altogether around $x = 2$. This is compatible with the following coarse estimate of the decay of G'' beyond the maximum: For sufficiently large strain amplitudes γ, the system is expected to flow essentially all the time. If the shear rate $\dot{\gamma}$ changes sufficiently slowly ($\omega \ll 1$), the stress can be approximated as following ''adiabatically'' the instantaneous shear rate: $\sigma(t) \approx \sigma(\dot{\gamma}(t))$ with $\sigma(\dot{\gamma})$ the steady shear flow curve. For $1 < x < 2$ and sufficiently small shear rates $\gamma\omega$, we know from Sec. V A that this relationship is a power law, $\sigma(\dot{\gamma}) \sim \dot{\gamma}^{x-1}$. Hence $\sigma(t) \sim (\gamma\omega\sin\omega t)^{x-1}$, which leads to a γ dependence of $G'' \sim \gamma^{x-2}$. For $x \to 2$, G'' should therefore no longer decay for large γ (as long as the condition $\gamma\omega \ll 1$ is obeyed), in agreement with our observation that its maximum with respect to γ disappears around this value of x. The estimate $G'' \sim \gamma^{2-x}$ is roughly compatible with our numerical data, but a precise verification of this power law is difficult (due to severe numerical problems for $\gamma \geqslant 20$). Note that within the same approximation, G' would be estimated to be identically zero, which is of course unphysical. Instead, we expect it to decay to zero faster than G'' as γ increases, and this is indeed what our numerical data show.

2. Size of linear regime

The above results allow us to determine the size of the linear regime for oscillatory rheological measurements, i.e., the largest strain amplitude γ_c for which the measured values of G' and G'' represent the linear response of the system. An important first observation that can be made on the basis of Fig. 16 is that the size of the residual r is not in general sufficient to determine whether one is in the linear regime or not. For example, for strain amplitude $\gamma = 1.5$ at $x = 1.1$ and $\omega = 0.1$, r is only around 2.5% even though the value of G'' is already twice as large as in the linear regime. The $\sigma(t)$ vs $\gamma(t)$ plot in Fig. 15(b) also demonstrates this: for $\gamma = 1.5$, the curve still looks almost perfectly elliptical, suggesting linear response, while its axis ratio is actually quite different from the one in the linear regime. Closer to the glass transition,

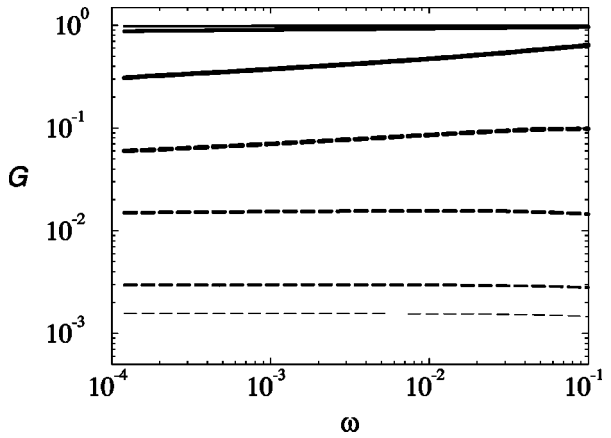

FIG. 17. Frequency dependence of (nonlinear) dynamic moduli $G'(\omega,\gamma)$ (solid lines) and $G''(\omega,\gamma)$ (dashed) measured at constant finite strain amplitude γ. Noise temperature $x=1.001$; increasing values of $\gamma=0$, 1, 2, 3 correspond to increasing line thickness. Recall that γ is rescaled by a typical local yield strain; $\gamma=1$ therefore corresponds to a real strain of at most a few percent. The loss modulus G'' increases strongly with γ, whereas G' varies much less (the curves for $\gamma=0$ and $\gamma=1$ cannot even be distinguished on the scale of the plot).

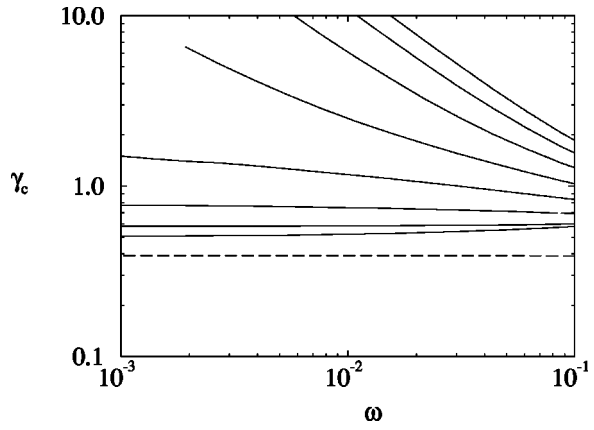

FIG. 18. Size of linear regime γ_c vs ω for $x=1.001$, 1.5, 2, . . . , 5 (bottom to top on left). Close to the glass transition, deviations from linearity first show up in G'', which therefore determines γ_c (dashed line); for larger x, the linear regime is limited by deviations in G' (solid lines). Recall that γ_c, like all strain variables, is rescaled by a typical local yield strain; $\gamma_c=1$ therefore corresponds to a real strain of at most a few percent.

this effect becomes even more pronounced. It suggests strongly that whenever the dynamic moduli of SGMs are measured, an explicit strain sweep is needed to determine whether measurements are actually taken in the linear regime.

If concerns about nonlinear effects are disregarded, an experimentally convenient procedure is to measure the dynamic moduli at fixed strain amplitude γ (while varying the frequency ω). Some numerical results for this case are shown in Fig. 17. Again, the most interesting behavior occurs near the glass transition. There, we observe that only relatively minor differences in the amplitude of the imposed strain can lead to large changes in the measured values of G'' (whereas G' is affected less strongly). This emphasizes again that extreme caution needs to be taken in experiments designed to determine the dynamic moduli of soft glassy materials; in particular, it needs to be borne in mind that the loss modulus can easily be overestimated due to undetected nonlinear effects.

Finally, the actual size of the linear regime itself is also of interest. We choose as a working definition of the linear regime the strain amplitude γ_c at which either G' or G'' first deviate by 10% from their values in the limit $\gamma\to 0$. (This implies similar maximum relative deviations for $|G^*|$ and the loss tangent $\tan\delta=G''/G'$.) Figure 18 shows $\gamma_c(\omega)$ for several noise temperatures x. Several general trends can clearly be read off. First, in the low frequency regime, the size of the linear regime decreases as the glass transition is approached. This is intuitively reasonable as one expects nonlinearities to become stronger near the glass transition [64]. Note, however, that γ_c does not decrease to zero at the glass transition; it tends to a finite value of order unity, which by our choice of units corresponds to the typical (*a priori*) yield stress of local elements. The frequency dependence of $\gamma_c(\omega)$ also changes as one moves away from the glass transition: Initially (for $x\approx 1$), γ_c is essentially independent of ω and does remain so until around $x=3$ (although its absolute value increases); for yet higher noise temperatures, one finds a crossover to a $\gamma_c\sim\omega^{-1}$ dependence. The latter corresponds to the ''naive'' criterion that the typical shear rate $\gamma\omega$ needs to be smaller than typical relaxation rates (of order unity away from the glass transition) in order for the imposed strain not to create nonlinear effects. The predicted ω independence of γ_c near the glass transition should be easy to verify experimentally.

VI. INTERPRETATION OF MODEL PARAMETERS

As has been demonstrated above, the SGR model captures important rheological features that have been observed in a large number of experiments, at least in the region around the ''glass transition'' of the model. Using a mean-field (one element) picture, it is also simple enough to be generic. However, a significant challenge that remains is the interpretation of the model parameters, namely, the ''effective noise temperature'' x and the ''attempt frequency'' Γ_0. To tackle these questions, we should really start from a more comprehensive model for the coupled nonlinear dynamics of the ''elements'' of a SGM and then derive the SGR model within some approximation scheme. At present, we do not know how to do this, and the following discussion will therefore have to remain rather speculative.

A. Effective noise temperature x

We can interpret the activation factor $\exp[-(E-\frac{1}{2}kl^2)/x]$ in the equation of motion (3) of the SGR model as the probability that (within a time interval of order $1/\Gamma_0$) a given element yields due to a ''kick'' from a rearrangement (yield event) elsewhere in the material. Therefore x is the typical activation energy available from such kicks. But while kicks can *cause* rearrangements, they also *arise* from rearrangements (whose effects, due to interactions, propagate through the material). So there is no separate energy scale for kicks: Their energy must of the order of the energies released in rearrangements, i.e., of the order of typical yield energies E.

In our units, this means that x should be of order unity. Note that this is far bigger than what we would estimate if x represented true thermal activation. For example, the activation barrier for the simplest local rearrangement in a foam (a $T1$ or neighbor-switching process) is of the order of the surface energy of a single droplet; this sets our basic scale for the yield energies E. Using typical values for the surface tension and a droplet radius of the order of 1 μm or greater, we find $E \gtrsim 10^4 k_B T$. In our units $E = O(1)$, so thermal activation would correspond to extremely small values of $x = k_B T \lesssim 10^{-4}$.

We now argue that x may not only be of order one, but in fact close to one generically. Consider first a steady shear experiment. The rheological properties of a sample freshly loaded into a rheometer are usually not reproducible; they become so only after a period of shearing to eliminate memory of the loading procedure. In the process of loading one expects a large degree of disorder to be introduced, corresponding to a high noise temperature $x \gg 1$. As the sample approaches the steady state, the flow will (in many cases) tend to eliminate much of this disorder [65] so that x will decrease. But, as this occurs, the noise-activated processes will slow down; as $x \to 1$, they may become negligible. Assuming that, in their absence, the disorder cannot be reduced further, x is then ''pinned'' at a steady-state value at or close to the glass transition. This scenario, although extremely speculative, is strongly reminiscent of the ''marginal dynamics'' seen in some mean-field spin glass models. In the spherical p-spin glass, for example, one finds that after a quench from $T = \infty$ to *any* temperature $0 < T < T_g$ below the (dynamical) glass transition temperature T_g, the system is dynamically arrested in regions of phase space characteristic of T_g itself, rather than the true temperature T [44,45].

There remain several ambiguities within this picture, for example, whether the steady state value of x should depend on $\dot{\gamma}$; if it does so strongly, our results for steady flow curves will of course be changed. If a steady flow is stopped and a linear viscoelastic measurement performed, the results should presumably pertain to the x characterizing the preceding steady flow (assuming that x reflects structure only). But unless the strain amplitude is extremely small the x value obtained in the steady state could be affected by the oscillatory flow itself. This might allow ''flat'' moduli $G^*(\omega)$ ($x \approx 1$) to be found alongside a nonzero yield stress with power-law flow exponent around 1/2 ($x \approx 1/2$) [7,43,66].

Experimentally, the above ideas concerning the time evolution of x in steady flows could be tested in systems that can be prepared in both low- and high-disorder states, such as onion phases [67]: Strain induced ordering starting from an initial x well below or above $x_g = 1$ should drive the system towards $x = 0$ or $x \approx 1$, respectively, leading to different rheological characteristics.

Theoretically, the minimal extension to the SGR model that would be needed to substantiate the above scenario would be to allow x to evolve in time. We do not know at present how to deduce the correct form of this evolution in a principled way from some underlying microscopic dynamics. However, one possibility is to couple x to the number of rearrangements in the material, i.e., the yielding rate Γ. Indeed, suppose we view Γ_0^{-1} as a memory time during which an element accumulates kicks before attempting a rearrangement. The number of kicks accumulated is then proportional to Γ/Γ_0. If individual kicks are thought of as independent Gaussian perturbations, and we identify x with the mean-squared size of the ''cumulative'' kick, then $x = A\Gamma/\Gamma_0$. The proportionality constant A would depend, for example, on how kicks propagate through the system. For $\Gamma/\Gamma_0 = 1$, each element yields once (on average) within a time interval Γ_0^{-1}; A can therefore be viewed as the average number of kicks caused by a rearrangement. We leave the analysis of such an approach for future work; preliminary investigations suggest the emergence of interesting features such as bistable solutions for the flow curve $\sigma(\dot{\gamma})$.

B. Attempt frequency Γ_0

Consider now the attempt frequency Γ_0. It is the only source of a characteristic time scale in our model (chosen as the time unit above). This excludes a naive proposal for the origin of Γ_0: The attempt frequency cannot be derived (in some self-consistent way) from the yielding rate Γ, because the model would then no longer contain an intrinsic time scale. This would imply that all dependencies on frequency or time are trivial, leading to unphysical results [the flow curves $\sigma(\dot{\gamma})$ would simply be a constant, as would be the linear moduli $G'(\omega)$ and $G''(\omega)$].

We have so far approximated Γ_0 by a constant value, independently of the shear rate $\dot{\gamma}$; this implies that Γ_0 is not caused by the flow directly. One possibility, then, is that Γ_0 arises in fact from *true* thermal processes, i.e., rearrangements of very ''fragile'' elements with yield energies of order $k_B T$. To a first approximation, such processes could be accounted for by extending the basic equation of motion (3) to

$$\frac{\partial}{\partial t} P(E,l,t) = -\dot{\gamma}\frac{\partial}{\partial l} P - \Gamma_{\rm th}\, e^{-[E-(1/2)kl^2]/k_B T}\, P - \Gamma_0\, e^{-[E-(1/2)kl^2]/x}\, P + \Gamma(t)\rho(E)\delta(l). \tag{32}$$

Here $\Gamma_{\rm th}$ is an attempt rate for true thermal processes, which should be a local diffusion rate. In emulsions with μm droplets, typical rates for such diffusive modes could be of the order of 1–100 Hz [11]. The term on the rhs of Eq. (32) proportional to $\Gamma_{\rm th}$ corresponds to yield events caused directly by thermal fluctuations. Due to the presence of interactions between the different elements of the material, the effects of such yield events can propagate through the system and cause other rearrangements. These are described by the term proportional to Γ_0. The ''attempt frequency'' Γ_0 is now no longer an independent parameter; instead, it is proportional to the average rate of thermal rearrangements,

$$\Gamma_0 = A\langle \Gamma_{\rm th}\, e^{-[E-(1/2)kl^2]/k_B T}\rangle_P .$$

The ''propagation factor'' A again represents the number of kicks caused by a thermally induced yield event. It has a crucial effect on the behavior of the modified model (32), as

can be seen by considering the equilibrium distribution in the absence of macroscopic strain [$\gamma(t)=0$]. One has $P_{\rm eq}(E,l)=P_{\rm eq}(E)\,\delta(l)$ with

$$P_{\rm eq}(E)=\frac{\Gamma}{\Gamma_{\rm th}e^{-E/k_{\rm B}T}+\Gamma_0 e^{-E/x}}\rho(E).$$

When Γ_0 is of the order of $\Gamma_{\rm th}$ or larger, $P_{\rm eq}(E)\propto\exp(E/x)\rho(E)$ as in the original version (3) of the model. From this, the value of Γ_0 can be calculated; for the assumption $\Gamma_0\gtrsim\Gamma_{\rm th}$ to be self-consistent, one then requires

$$\frac{\Gamma_0}{\Gamma_{\rm th}}=A\frac{\int dE\ \rho(E)\exp(-E/k_{\rm B}T)}{\int dE\ \rho(E)\exp(E/x)}\gtrsim 1 \qquad (33)$$

(here we have neglected a term E/x in the exponent of the numerator because $k_{\rm B}T\ll x$). This condition can be given an intuitive interpretation: A must be large enough for each thermal yield event to produce at least one new element that can yield thermally (i.e., whose yield energy E is of order $k_{\rm B}T$), thus maintaining the population of such fragile elements. For smaller A, one finds instead that $\Gamma_0/\Gamma_{\rm th}\sim\exp(-\overline{E}/k_{\rm B}T)$, which for typical barrier energies $\overline{E}=O(1)$ (in our units) is unfeasibly slow. The above mechanism can therefore give a plausible rheological time scale *only* if the average number A of rearrangements triggered by one local, thermally induced rearrangement is large enough to sustain the population of fragile elements, as determined by Eq. (33). The values of A actually required for this are sensitive to the small E behavior of $\rho(E)$. Assuming, for example, $\rho(E)\propto E^{y-1}\exp(-E)$, one has the condition

$$A\gtrsim[k_{\rm B}T(1-x^{-1})]^{-y}.$$

For $y=1$, where $\rho(E)$ stays finite for $E\to 0$, this requires at least $A\gtrsim 10^4$. Such large values appear implausible unless a single yield event could trigger a whole ''avalanche'' of others; in foams, it has been argued that this might be the case [21]. On the other hand, significantly smaller values of A would be sufficient if $\rho(E)$ shows a significant bias towards small yield energies E ($0\approx y<1$). The above ''thermal trigger'' scenario would then be more generically plausible. To draw more definite conclusions on this point, it would be useful to measure $\rho(E)$ in, for example, a computer simulation of a model SGM.

There are a number of other possible explanations for the origin of Γ_0. These include, for example, noise sources internal to the material, such as coarsening in a foam, or uncontrolled external noise. Finally, the rheometer itself could also be a potential source of noise; this would, however, suggest at least a weak dependence of Γ_0 on the shear rate $\dot\gamma$. We cannot at present say which of these possibilities is most likely, nor rule out other candidates. The origin of Γ_0 may not even be universal, but could be system specific.

VII. CONCLUSION

We have solved exactly the SGR (soft glassy rheology) model of Ref. [17] for the low frequency shear rheology of materials such as foams, emulsions, pastes, slurries, etc. The model focuses on the shared features of such soft glassy materials (SGMs), namely, structural disorder and metastability. These are built into a generic description of the dynamics of mesoscopic elements, with interactions represented by a mean-field noise temperature x. All rheological properties can be derived from an exact constitutive equation.

In the linear response regime, we found that both the storage modulus G' and the loss modulus G'' vary with frequency as ω^{x-1} for $1<x<2$. Near the glass transition, they become flat, in agreement with experimental observations on a number of materials. In the glass phase, the moduli are predicted to *age*; this could provide an interesting experimental check of the model.

Far above the glass transition, the steady shear behavior is Newtonian at small shear rates. Closer to the transition ($1<x<2$), we found power-law fluid behavior; in the glass phase, there is an additional nonzero yield stress (Herschel-Bulkley model). The last two regimes therefore capture important features of experimental data. Above the glass transition, the validity of the Cox-Merz rule relating the frequency dependence of the linear moduli to the shear viscosity can be checked; it breaks down in the power-law fluid region and fails spectacularly at the glass transition. In this regime, stress overshoots in shear startup are strongest. We have also calculated the distribution of energies dissipated in local yield events. At variance with existing simulation data for foams, this exhibits a shear-rate dependent crossover between two power-law regimes; this discrepancy remains to be resolved.

We further probed the nonlinear behavior of the model by considering large amplitude single and double step strains. The nonlinear response cannot in general be factorized into strain and time dependent terms, and is not well represented by the BKZ equation. Finally, we considered measurements of G' and G'' in oscillatory strain of finite amplitude γ. Near the glass transition, G'' exhibits a maximum as γ is increased (strain sweep), reproducing qualitative features of recent measurements on emulsions and colloidal glasses. The contribution of higher harmonics to the stress response is not always sufficient to determine whether the response is nonlinear, emphasizing the need for explicit strain sweeps to get reliable data in the linear regime. Otherwise, measurements at constant strain amplitude can lead to strongly enhanced values of the loss modulus G''. Finally, we considered the size of the linear regime itself, i.e., the largest strain amplitude γ_c at which the measured values of G' and G'' still represent the linear response of the system. The SGR model predicts that γ_c should be roughly frequency independent near the glass transition; this point should also be amenable to experimental verification.

In the final section, we speculated on the physical origin of the most important parameters of the model, namely, the effective temperature x and the attempt frequency for rearrangements Γ_0. We argued that x should be generically of order unity (in our units). This is because it represents the typical energy released in a rearrangement, which is of the same order as the activation energy required to cause a rearrangement elsewhere in the material. A speculative analogy to marginal dynamics in other glassy systems suggests that x

may in fact be close to unity in general. This is encouraging, because the SGR model reproduces the qualitative features of experimental data best for $x \approx 1$, i.e., near the glass transition. We mentioned several hypotheses for the origin of the attempt frequency Γ_0, which include events triggered by thermal fluctuations or internal and external noise sources not explicitly contained within the model.

In future work, we plan to explore in more detail the strongly history-dependent behavior of the model in the glass phase. Its simplicity should allow this to be done in detail, thereby providing the first full theoretical study to be made of the generic relationship between aging and rheology [47]. Apart from this, the main challenge is to incorporate spatial structure and explicit interactions between elements into the model. This should help us understand better the mutual dynamical evolution of the attempt rate, the effective noise temperature and the structural disorder. In the end, one would hope to derive a model similar to the present one from such a more microscopic description within some well-defined approximation scheme.

ACKNOWLEDGMENTS

The author is indebted to F. Lequeux, P. Hébraud, and M. E. Cates for their significant contributions to the development and initial investigation of the SGR model, as published in Ref. [17], and for helpful comments on the present manuscript. Thanks are due also to J.-P. Bouchaud for several seminal suggestions. Financial support from the Royal Society of London, and from the National Science Foundation under Grant No. PHY94-07194, is gratefully acknowledged.

APPENDIX A: DERIVATION OF CONSTITUTIVE EQUATION

The equation of motion (3) of the SGR model can be solved by making the time dependent change of variable $l \rightarrow \Delta l = l - \gamma(t)$. This eliminates the $\dot{\gamma}$ (convective) term, converting the equation of motion from a PDE to an ODE. Suppressing the E and Δl dependence of P, the result reads

$$\frac{\partial}{\partial t}P(t) = -\exp\left\{-\frac{1}{x}[E - \tfrac{1}{2}(\Delta l + \gamma(t))^2]\right\}P(t) + \Gamma(t)\rho(E)\,\delta(\Delta l + \gamma(t)).$$

This can be integrated to give

$$P(t) = P(0)\exp[-e^{-E/x}z(t,0;\Delta l)] + \int_0^t dt'\,\Gamma(t')\rho(E)\,\delta(\Delta l + \gamma(t')) \times \exp[-e^{-E/x}z(t,t';\Delta l)] \quad \text{(A1)}$$

with the auxiliary function

$$z(t,t';\Delta l) = \int_{t'}^t dt'' \exp\{[\Delta l + \gamma(t'')]^2/2x\}.$$

To simplify matters, we now assume that the initial ($t=0$) state is completely unstrained, i.e., $\gamma(0)=0$ and $P(0) = P_0(E)\delta(l) = P_0(E)\delta(\Delta l)$. The stress can be calculated by multiplying (A1) by Δl and integrating over E and Δl:

$$\sigma(t) = \gamma(t) + \langle \Delta l \rangle_{P(t)} = \gamma(t) - \int_0^t dt'\,\Gamma(t')\,\gamma(t') \int dE\ \rho(E) \times \exp[-e^{-E/x}z(t,t';-\gamma(t'))]. \quad \text{(A2)}$$

Here the yielding rate $\Gamma(t)$ is still undetermined, but it can be gotten from the condition of conservation of probability: The integral of Eq. (A1) over E and Δl has to be equal to unity, hence,

$$1 = \int dE\ P_0(E)\exp[-e^{-E/x}z(t,0;0)] + \int_0^t dt'\,\Gamma(t') \int dE\ \rho(E) \times \exp[-e^{-E/x}z(t,t';-\gamma(t'))]. \quad \text{(A3)}$$

To write the results (A2) and (A3) in a more compact form, the auxiliary functions defined in Eq. (11) and the abbreviation (12)

$$Z(t,t') = z(t,t';-\gamma(t')) = \int_{t'}^t dt'' \exp\{[\gamma(t'') - \gamma(t')]^2/2x\}$$

are used. This yields directly Eq. (10) for the yielding rate $\Gamma(t)$, while for the stress one obtains

$$\sigma(t) = \gamma(t) - \int_0^t dt'\,\Gamma(t')\,\gamma(t')\,G_\rho(Z(t,t')). \quad \text{(A4)}$$

This can be expressed in the more suggestive form (9) by writing the first term on the rhs as $\gamma(t)$ times the rhs of Eq. (10).

APPENDIX B: ASYMPTOTIC BEHAVIOR OF $G_\rho(z)$

In this appendix, we derive the asymptotic behavior (13) of $G_\rho(z)$. As explained in Sec. III, our choice of units $x_g = 1$ implies $\rho(E) = \exp\{-E[1+f(E)]\}$ with $f(E) \rightarrow 0$ for $E \rightarrow \infty$. Hence for any $\delta > 0$, there exists $M > 0$ such that $|f(E)| < \delta$ for $E > M$. Our strategy will be to split the defining integral (11) for $G_\rho(z)$ into two parts, for energies above and below the threshold M and to bound these separately. Writing

$$G_\rho(z) = \int_0^M dE\ \rho(E)\exp(-ze^{-E/x}) + \int_M^\infty dE\ \rho(E)\exp(-ze^{-E/x})$$

the first term on the rhs is trivially bounded by zero from below and by $\exp[-z\exp(-M/x)]$ from above. The second term, on the other hand, is bracketed by

$$\int_M^\infty dE\ e^{-(1\pm\delta)E}\exp(-ze^{-E/x})$$

$$=xz^{-x(1\pm\delta)}\int_0^{ze^{-M/x}} dy\ y^{x(1\pm\delta)-1}e^{-y} \qquad \text{(B1)}$$

(the plus and minus sign giving the lower and upper bound, respectively). Now consider the behavior of $G_\rho(z)z^{x+\epsilon}$ for some arbitrary small $\epsilon>0$. Choose $\delta=\epsilon/(2x)$ and a corresponding M; then from Eq. (B1)

$$G_\rho(z)z^{x+\epsilon}>xz^{\epsilon/2}\int_0^{ze^{-M/x}} dy\ y^{x+\epsilon/2-1}e^{-y}.$$

The integral has a finite limit for $z\to\infty$ (it is just a Gamma function), and so this lower bound tends to infinity in this limit, proving the first part of Eq. (13). The second part is demonstrated in a similar fashion: with the same choice of δ for a given ϵ, and again using (B1),

$$G_\rho(z)z^{x-\epsilon} < z^{x-\epsilon}\exp(-ze^{-M/x}) + xz^{-\epsilon/2}\int_0^{ze^{-M/x}} dy\ y^{x-\epsilon/2-1}e^{-y}.$$

Again, the integral has a finite limit (assuming ϵ is sufficiently small, i.e., $\epsilon<2x$), and both terms on the rhs therefore tend to zero for $z\to\infty$, completing the proof of Eq. (13).

APPENDIX C: FLOW CURVES AND YIELD STRESS

Here we derive the small shear rate behavior of the flow curves $\sigma(\dot\gamma)$. As shown in Sec. V A, the stress $\sigma(\dot\gamma)=I_1(\dot\gamma)/I_0(\dot\gamma)$ can be expressed in terms of the functions

$$I_n(\dot\gamma)=\int_0^\infty dl\ l^n G_\rho(Z(l)). \qquad \text{(C1)}$$

The scaling of I_n with $\dot\gamma$ can be obtained from the asymptotic behavior of $G_\rho(z)$. From (13), it follows that for any $\epsilon>0$, we can choose a z_0 such that

$$z^{-x-\epsilon}<G_\rho(z)<z^{-x+\epsilon} \ \text{ for } z>z_0. \qquad \text{(C2)}$$

Now we use z_0 to decompose the l integral in Eq. (C1) into the parts with $l\lessgtr z_0\dot\gamma$:

$$I_n=I_n^<+I_n^>, \quad I_n^<=\int_0^{z_0\dot\gamma} dl\ l^n G_\rho(Z(l)).$$

Replacing $G_\rho(Z(l))$ by its minimum and maximum over the integration range, $I_n^<$ is trivially bounded by

$$G_\rho(Z(z_0\dot\gamma)) < \frac{n+1}{(z_0\dot\gamma)^{n+1}} I_n^< < A1.$$

As $\dot\gamma\to0$, the lhs tends to $G_\rho(z_0)$, so we have the scaling $I_n^<=O(\dot\gamma^{n+1})$. To bound $I_n^>$, we use that $Z(l)>l/\dot\gamma>z_0$ in the relevant integration range, so that the bounds (C2) on G_ρ can be used. Writing $Z(l)$ out explicitly, this gives lower and upper bounds for $I_n^>$ of

$$\dot\gamma^{x\mp\epsilon}\int_{z_0\dot\gamma}^\infty dl\ l^n\left(\int_0^l d\gamma\ e^{\gamma^2/2x}\right)^{-x\pm\epsilon}.$$

For $x<n+1$ (and ϵ sufficiently small), the outer integral has a finite limit for $\dot\gamma\to0$, and so $I_n^>$ scales as $\dot\gamma^x$ up to sub-power-law factors. For larger values of x, on the other hand, this integral diverges as $\dot\gamma^{n+1-x\pm\epsilon}$. $I_n^>$ then scales as $\dot\gamma^{n+1}$ (since both the lower and upper bound do), i.e., in the same way as $I_n^<$.

As discussed in Sec. V A, the above scaling properties of $I_n^<$ and $I_n^>$ prove that the flow curve is a power law $\sigma\sim\dot\gamma^{x-1}$ (up to sub-power-law factors) in the regime $1<x<2$. In the glass phase ($x<1$), the simplest case is that of exponential $\rho(E)$ [Eq. (7)]. The asymptotic behavior $G_\rho(z)\sim z^{-x}$ then translates directly into $I_n^>\sim\dot\gamma^x$ without sub-power-law corrections, and this gives the Herschel-Bulkley form (24) of the flow curve. The yield stress (25) is given by the limit of $I_1^>/I_0^>$ for $\dot\gamma\to0$, while the power-law onset of the additional stress arises from the small corrections due to $I_0^<$.

For general $\rho(E)$, on the other hand, the sub-power-law factors in $I_n^>(\dot\gamma)$ cause a corresponding weak $\dot\gamma$ dependence of $\sigma(\dot\gamma)$, which dominates the effect of the small correction terms $I_n^<(\dot\gamma)$. The flow curve therefore no longer has the simple Herschel-Bulkley form (24). However, in the examples that we tested numerically [$\rho(E)\sim E^n\exp(-E)$ for $n=1, 2, 3$], we found that this form still provides a good fit to $\sigma(\dot\gamma)$ over several decades of shear rate $\dot\gamma$. Both the exponent and yield stress of such a fit are then only effective quantities and depend on the range of $\dot\gamma$ considered; they are therefore no longer directly related to x. In the examples that we studied, we always found values of the effective exponent significantly below unity.

The slow sub-power-law variation of $\sigma(\dot\gamma)$ for general $\rho(E)$ means that there is, for practical purposes, always an effective yield stress (whose actual value depends weakly on the lowest accessible shear rate $\dot\gamma$). Nevertheless, one may wonder what the ''true'' yield stress $\sigma_y=\sigma(\dot\gamma\to0)$ would be. The above line of argument does not answer this question; it does not even exclude the possibility of σ_y being zero. We have examined this issue for several different sub-power-law corrections to the asymptotic behavior of G_ρ, such as $G_\rho(z)z^x\sim(\ln z)^m$, or $\sim\exp[(\ln z)^n]$ with $|n|<1$. The yield stress is always nonzero, and in fact turns out to be the same as for exponential $\rho(E)$. We suspect that this may be true in general, but have not found a proof.

APPENDIX D: NUMERICAL DETERMINATION OF $G^*(\omega,\gamma)$

In this appendix, we outline the numerical scheme that we used to obtain the nonlinear dynamic modulus $G^*(\omega,\gamma)$ and the residual r defined in Eqs. (30) and (31), respectively. As explained in Sec. V D, we are interested in the steady state

stress response in the ergodic regime $x>1$. We can then safely send the initial time to $-\infty$ in the CE (9) and (10). The equations that need to be solved can be simplified further by using the fact that in the steady state, the yielding rate $\Gamma(t)$ must have the same periodicity as the applied strain $\gamma(t)$. Denoting the oscillation period by $T=2\pi/\omega$, the task is then to solve

$$1=\int_{t-T}^{t} dt'\Gamma(t')H(t,t') \tag{D1}$$

for $\Gamma(t)$ and then to evaluate the stress from

$$\sigma(t)=\gamma(t)-\int_{t-T}^{t} dt'\,\gamma(t')\Gamma(t')H(t,t'). \tag{D2}$$

Here the periodicity of the problem has been absorbed into the definition of

$$H(t,t')=\sum_{n=0}^{\infty} G_\rho(Z(t,t'-nT))$$

$$=\sum_{n=0}^{\infty} G_\rho(Z(t,t')+nZ(t'+T,t')),$$

where the second equality follows again from the periodicity of the strain $\gamma(t)=\gamma\cos\omega t$. The numerical solution of the integral equation (D1) is simplified by subtracting from the kernel $H(t,t')$ a part that depends on t' only:

$$\tilde{H}(t,t')=H(t,t')-H(t'+T,t')=\left\langle \frac{e^{-\Omega Z_1}-e^{-\Omega Z_2}}{1-e^{-\Omega Z_2}}\right\rangle_\rho ,$$

where we have abbreviated $\Omega=\exp(-E/x)$, $Z_1=Z(t,t')$, $Z_2=Z(t'+T,t')$. The modified kernel $\tilde{H}(t,t')$ has the convenient properties $\tilde{H}(t',t')=1$, $\tilde{H}(t'+T,t')=0$ and is also simpler to evaluate numerically than $H(t,t')$. The yielding rate can easily be calculated from $\tilde{H}$ instead of H: Defining a modified yielding rate $\tilde{\Gamma}(t)$ as the solution of

$$1=\int_{t-T}^{t} dt'\tilde{\Gamma}(t')\tilde{H}(t,t') \tag{D3}$$

the actual yielding rate is recovered by dividing by the constant factor

$$1+\int_0^T dt'\tilde{\Gamma}(t')H(t'+T,t').$$

However, even the solution of Eq. (D3) is still nontrivial, especially in the low frequency regime $T\gg 1$ that we are most interested in. This is because $\tilde{H}$ ''inherits'' from G_ρ an initial ''fast'' decay as $t-t'$ increases from zero, followed by a much slower power-law decay (which in turn gives way to a rapid final decay as soon as strain-induced yielding becomes important). This separation of $O(1)$ and $O(T)$ time scales rules out traditional solution methods such as Chebyshev approximation. Instead, we solve Eq. (D3) by Fourier transform: Writing

$$\tilde{\Gamma}(t)=\sum_{n=-\infty}^{\infty}\tilde{\Gamma}_n e^{in\omega t}$$

Eq. (D3) is transformed into the matrix equation

$$\sum_{m=-\infty}^{\infty}\tilde{H}_{nm}\tilde{\Gamma}_m=\delta_{n,0} \tag{D4}$$

with coefficients

$$\tilde{H}_{mn}=\int_0^T\frac{dt}{T}e^{-i(n-m)\omega t}\int_0^T d\tau\, e^{-im\omega\tau}\tilde{H}(t,t-\tau).$$

Once Eq. (D4) is solved and the rescaling from $\tilde{\Gamma}$ to Γ is carried out, the stress is obtained as

$$\frac{\sigma(t)}{\gamma}=\sum_n \sigma_n e^{in\omega t},$$

$$\sigma_n=\frac{1}{2}(\delta_{n,-1}+\delta_{n,1})-\frac{1}{2}\sum_m \Gamma_m(\tilde{H}_{n,m+1}+\tilde{H}_{n,m-1}).$$

Its Fourier components determine the nonlinear dynamic modulus and squared residual as

$$G^*(\omega,\gamma)=2\sigma_1 \qquad r^2=1-\frac{|\sigma_1|^2}{\sum_{k=0}^{(\infty)}|\sigma_{2k+1}|^2}.$$

The result for r^2 has been simplified using the fact that $\sigma_{-n}=\sigma_n^*$ [because $\sigma(t)$ is real] and that $\sigma_n=0$ for even n [because $\sigma(t)\to-\sigma(t)$ for $\gamma\to-\gamma$, which corresponds to $t\to t+T/2$].

To solve the main equation (D4), we truncate the matrix equation at successively higher orders until the calculated values of $G'(\omega,\gamma)$, $G''(\omega,\gamma)$, and r are stable to within 1%. The Fourier components $\tilde{H}_{mn}$ are calculated from a spline interpolant approximation to $\tilde{H}(t,t')$ in order to save expensive function evaluations.

[1] S. D. Holdsworth, Trans. Inst. Chem. Eng. **71**, 139 (1993).
[2] E. Dickinson, *An Introduction to Food Colloids* (Oxford University Press, Oxford, 1992).
[3] H. A. Barnes, J. F. Hutton, and K. Walters, *An Introduction to Rheology* (Elsevier, Amsterdam, 1989).
[4] M. R. Mackley, R. T. J. Marshall, J. B. A. F. Smeulders, and F. D. Zhao, Chem. Eng. Sci. **49**, 2551 (1994).
[5] R. J. Ketz, R. K. Prudhomme, and W. W. Graessley, Rheol. Acta **27**, 531 (1988).
[6] S. A. Khan, C. A. Schnepper, and R. C. Armstrong, J. Rheol. **32**, 69 (1988).
[7] T. G. Mason, J. Bibette, and D. A. Weitz, Phys. Rev. Lett. **75**, 2051 (1995).
[8] P. Panizza, D. Roux, V. Vuillaume, C. Y. D. Lu, and M. E. Cates, Langmuir **12**, 248 (1996).
[9] H. Hoffmann and A. Rauscher, Colloid Polymer Sci. **271**, 390 (1993).
[10] T. G. Mason and D. A. Weitz, Phys. Rev. Lett. **75**, 2770 (1995).
[11] D. M. A. Buzza, C. Y. D. Lu, and M. E. Cates, J. Phys. II **5**, 37 (1995).
[12] J. P. Bouchaud, J. Phys. I **2**, 1705 (1992).
[13] C. Monthus and J. P. Bouchaud, J. Phys. A **29**, 3847 (1996).
[14] J. P. Bouchaud and D. S. Dean, J. Phys. I **5**, 265 (1995).
[15] V. M. Vinokur, M. C. Marchetti, and L. W. Chen, Phys. Rev. Lett. **77**, 1845 (1996).
[16] P. LeDoussal and V. M. Vinokur, Physica C **254**, 63 (1995).
[17] P. Sollich, F. Lequeux, P. Hébraud, and M. E. Cates, Phys. Rev. Lett. **78**, 2020 (1997).
[18] Soft systems may also be intrinsically metastable in a more drastic sense (for example, with respect to coalescence in emulsions)—we ignore this here.
[19] D. Weaire and M. A. Fortes, Adv. Phys. **43**, 685 (1994).
[20] M. D. Lacasse, G. S. Grest, D. Levine, T. G. Mason, and D. A. Weitz, Phys. Rev. Lett. **76**, 3448 (1996).
[21] T. Okuzono and K. Kawasaki, Phys. Rev. E **51**, 1246 (1995).
[22] D. J. Durian, Phys. Rev. Lett. **75**, 4780 (1995).
[23] D. J. Durian, Phys. Rev. E **55**, 1739 (1997).
[24] J. P. Bouchaud, A. Comtet, and C. Monthus, J. Phys. I **5**, 1521 (1995).
[25] T. Odagaki, J. Matsui, and Y. Hiwartari, Physica A **204**, 464 (1994).
[26] V. I. Arkhipov and H. Bässler, J. Phys. Chem. **98**, 662 (1994).
[27] R. Richert and H. Bässler, J. Phys.: Condens. Matter **2**, 2273 (1990).
[28] T. A. Vilgis, J. Phys.: Condens. Matter **2**, 3667 (1990).
[29] H. Bässler, Phys. Rev. Lett. **58**, 767 (1987).
[30] J. W. Haus and K. W. Kehr, Phys. Rep. **150**, 263 (1987).
[31] W. Götze, in *Liquids, Freezing and Glass Transition*, edited by J. P. Hansen, D. Levesque, and J. Zinn-Justin (North-Holland, Amsterdam, 1991), pp. 287–503.
[32] W. Götze and L. Sjögren, Rep. Prog. Phys. **55**, 241 (1992).
[33] (Structural) glasses are often classified into ''strong'' and ''fragile'' glass formers (see, e.g., [68]). The former can be characterized, for example, by an Arrhenius dependence of the viscosity η on T temperature, while the latter show a much more dramatic variation of η with T near the glass transition. Mode-coupling theories generally predict fragile behavior, while trap models have been associated with strong glasses (see, e.g., [69]). The latter is only true for approximately uniform trap depths, however; indeed, we shall find within the SGR model a strongly non-Arrhenius dependence of η on the (noise) temperature x, due to a large spread of trap depths.
[34] It is always understood in the following that trap depths are restricted to positive values, $E>0$.
[35] J. P. Bouchaud and M. Mezard, J. Phys. A **30**, 7997 (1997).
[36] Precisely this motion is predicted, on a global rather than mesoscopic scale, for perfectly ordered foams (see, e.g., [70]).
[37] This constitutes a major difference between the SGR model and theories for the motion of elastic manifolds in random media: While both approaches describe flow in the presence of disorder, for elastic manifolds the *force F* driving the flow is assumed to be homogeneous throughout the sample (rather than the *strain rate*), and the distribution of trap depths has a cutoff whose strong dependence on F entirely dominates the low-temperature behavior (see, e.g., [15]).
[38] This picture should not be taken too literally, however; the SGR model does not retain any memory of the properties of the old well and the hop back will in general be to a well with a different depth. Bistable elements that oscillate between two (or a small finite number of) equilibrium states are therefore not well described by the model. Correlations between old and new well depths could be introduced to account for such effects. However, an explicit description in terms of two-state elements might be more appropriate where such effects are important. [M. L. Falk and J. S. Langer (unpublished).]
[39] Within mode-coupling theory, the fact that β relaxations correspond to localized motion—loosely describable as the rattling of particles in the cages formed by their neighbors ([32], p. 333)—has been deduced from the fact that correlation functions factorize into a time dependent and a separation (or wave vector) dependent part. Nevertheless, some degree of cooperative motion must be involved, at least on a local scale, because the motion of each particle within its cage affects the cages of its neighbors. The SGR model only captures the analog of the slower α relaxations, corresponding to the breakup of particle cages and structural rearrangements.
[40] This property of the model can be seen most clearly in the equilibrium state ($\dot{\gamma}=0$) for $x>1$. All elements are then unstrained, so both terms on the rhs of Eq. (6) are zero: The total elastic energy is constant (and equal to zero) and no energy is being dissipated. At the same time, however, rearrangements are predicted to occur at a finite rate Γ.
[41] This is true for a fixed distribution of yield energies $\rho(E)$, such as the one that we use in all our numerical work [$\rho(E)=\exp(-E)$]. In general, our choice of $x_g=1$ fixes only the asymptotic behavior $\rho(E)\sim\exp(-E)$, but not the details of the distribution of small yield energies E. These do affect the quantitative predictions of the SGR model, but do not alter qualitative features such as the power-law behavior of the shear moduli and flow curves.
[42] P. Hebraud, F. Lequeux, J. P. Munch, and D. J. Pine, Phys. Rev. Lett. **78**, 4657 (1997).
[43] T. G. Mason, J. Bibette, and D. A. Weitz, J. Colloid Interface Sci. **179**, 439 (1996).
[44] L. F. Cugliandolo and J. Kurchan, Phys. Rev. Lett. **71**, 173 (1993).

[45] L. F. Cugliandolo and J. Kurchan, Philos. Mag. B **71**, 501 (1995).
[46] The lower limit in the response integral (17) is zero rather than $-\infty$ because we assumed that the system is completely unstrained at $t=0$.
[47] P. Sollich and M. E. Cates (unpublished).
[48] In the large shear rate regime, the steady yielding rate Γ is found to be *greater* than the attempt frequency Γ_0. This is unphysical because a significant fraction of elements must then be yielding in the ''metastable'' regime $E-\frac{1}{2}l^2<0$, where the activation barrier for yielding is negative. For such negative barriers, the nominal yielding rate $\exp[-(E-\frac{1}{2}l^2)/x]$ actually increases rather than decreases with decreasing x; this causes a crossing of the flow curves at shear rates around $\dot{\gamma}=1$ (outside the range shown in Fig. 7). Such unphysical features could be avoided, for example, by fixing the yielding rate of an element to a constant (Γ_0, say) in the metastable regime (negative activation barrier). Unfortunately, this makes the model significantly harder to solve.
[49] T. Odagaki, Phys. Rev. Lett. **75**, 3701 (1995).
[50] W. P. Cox and E. H. Merz, J. Polym. Sci. **28**, 619 (1958).
[51] A. J. Liu, S. Ramaswamy, T. G. Mason, H. Gang, and D. A. Weitz, Phys. Rev. Lett. **76**, 3017 (1996).
[52] S. Hutzler, D. Weaire, and F. Bolton, Philos. Mag. B **71**, 277 (1995).
[53] A. D. Gopal and D. J. Durian, Phys. Rev. Lett. **75**, 2610 (1995).
[54] D. J. Durian, D. A. Weitz, and D. J. Pine, Science **252**, 686 (1991).
[55] J. C. Earnshaw and M. Wilson, J. Phys. II **6**, 713 (1996).
[56] For $\dot{\gamma}\gtrsim\sqrt{x}$, $P(\Delta E)$ can actually be nonmonotonic, with a maximum for values of ΔE of order unity. This is due to the yielding of elements from ''metastable'' states with $E-\frac{1}{2}l^2<0$.
[57] S. Tewari, D. Schiemann, D. J. Durian, S. A. Langer, and A. J. Liu (unpublished).
[58] The behavior in the glass phase ($x<1$) could be investigated by introducing an energy cutoff $E_{\max}$ as in Sec. IV B. However, the transient behavior $\sigma(t)$ turns out to be very sensitive to $E_{\max}$ (whereas the steady state stress is not) and is therefore of questionable significance.
[59] B. Bernstein, E. A. Kearsley, and L. J. Zapas, Trans. Soc. Rheol. **7**, 391 (1963).
[60] M. Doi and S. F. Edwards, *The Theory of Polymer Dynamics* (Clarendon Press, Oxford, 1986).
[61] M. Doi, J. Polym. Sci., Polym. Phys. Ed. **18**, 1891 (1980).
[62] T. G. Mason, M. D. Lacasse, G. S. Grest, D. Levine, J. Bibette, and D. A. Weitz, Phys. Rev. E **56**, 3150 (1997).
[63] P. Boltenhagen, J. Bibette, and F. Lequeux (unpublished).
[64] The observation of a decreasing γ_c as $x\rightarrow 1$ is nevertheless nontrivial. Naive arguments can easily be misleading: For example, one could argue incorrectly that, because the glass transition is caused by a strong increase in the fraction of elements with large yield energies E—and therefore large yield strains—γ_c should actually *increase* for $x\rightarrow 1$.
[65] D. Weaire, F. Bolton, T. Herdtle, and H. Aref, Philos. Mag. Lett. **66**, 293 (1992).
[66] H. M. Princen and A. D. Kiss, J. Colloid Interface Sci. **128**, 176 (1989).
[67] D. Roux (private communication).
[68] C. A. Angell, Science **267**, 1924 (1995).
[69] W. van Megen and S. M. Underwood, Phys. Rev. E **49**, 4206 (1994).
[70] A. M. Kraynik, Annu. Rev. Fluid Mech. **20**, 325 (1988).
[71] The corresponding curves in Ref. [17] (Fig. 2) contained a numerical error. However, this caused only slight changes in the quantitative details of the flow curves, without altering any of the qualitative conclusions (power laws, etc.).